

Turbofan Engine Sizing and Tradeoff Analysis via Signomial Programming

by

Martin A. York

B.S., Massachusetts Institute of Technology, 2017

Submitted to the Department of Aeronautics and Astronautics
in partial fulfillment of the requirements for the degree of

Master of Science in Aeronautics and Astronautics

at the

MASSACHUSETTS INSTITUTE OF TECHNOLOGY

June 2017

© Massachusetts Institute of Technology 2017. All rights reserved.

Author
Department of Aeronautics and Astronautics
May 25, 2017

Certified by.....
Warren W. Hoburg
Assistant Professor of Aeronautics and Astronautics
Thesis Supervisor

Accepted by.....
Youssef M. Marzouk
Associate Professor of Aeronautics and Astronautics
Chair, Graduate Program Committee

Turbofan Engine Sizing and Tradeoff Analysis via Signomial Programming

by

Martin A. York

Submitted to the Department of Aeronautics and Astronautics
on May 25, 2017, in partial fulfillment of the
requirements for the degree of
Master of Science in Aeronautics and Astronautics

Abstract

This thesis presents a full 1D core+fan flowpath turbofan optimization model, based on first principles, and meant to be used during aircraft conceptual design optimization. The model is formulated as a signomial program, which is a type of optimization problem that can be solved locally using sequential convex optimization. Signomial programs can be solved reliably and efficiently, and are straightforward to integrate with other optimization models in an all-at-once manner. To demonstrate this, the turbofan model is integrated with a simple commercial aircraft sizing model. The turbofan model is validated against the Transport Aircraft System OPTimization turbofan model as well as two Georgia Tech Numerical Propulsion System Simulation turbofan models. Four integrated engine/aircraft parametric studies are performed, including a 2,460 variable multi-mission optimization that solves in 28 seconds.

Thesis Supervisor: Warren W. Hoburg

Title: Assistant Professor of Aeronautics and Astronautics

Acknowledgments

I'd like to begin by thanking my family and friends for their support and comradery over the past five years. You helped me navigate the challenges of MIT while giving me some of my fondest memories. For this, I will always be grateful.

This thesis would not have been possible without the support and guidance of my research advisor, Professor Woody Hoburg, the work of lead GPkit developer Ned Burnell, and Professor Mark Drela. Woody is a superb research mentor and brilliant engineer. He introduced me to geometric and signomial programming while pushing me to develop the best research product I could. Ned's continued development and support of GPkit, as well as his willingness to assist whenever a software roadblock was encountered, were instrumental to the success of this work. Professor Drela's TASOPT provided the inspiration for this work and his technical feedback over the course of the project was invaluable.

I'd like to give a special thanks to my undergraduate advisor, Professor Sheila Widnall, who helped guide me through my unique five year SB/SM program as well as the cadre of Air Force ROTC Detachment 365, especially Lt Col Karen Dillard (Ret.) and Capt Peterson Dela Cruz, who enabled me to stay at MIT for a fifth year as a graduate student.

Finally, I would like to thank Aurora Flight Sciences for sponsoring this work.

Contents

1	Introduction	19
1.1	Optimization Formulation	20
1.1.1	Model Architecture	20
1.1.2	Solution Method	21
1.1.3	Geometric Programming	22
1.1.4	Signomial Programming	23
1.2	Terminology	24
1.2.1	Models	25
1.2.2	GP- and SP-compatibility	25
1.2.3	Static and Performance Models	26
2	Model Derivation	27
2.1	Combustor and Cooling Flow Mixing Model	28
2.2	Area, Mass Flow, and Speed Constraints	30
2.3	Fan and Compressor Maps	34
2.4	Exhaust State Model	39
2.5	Engine Weight	40
3	Model Validation	41
3.1	NPSS CFM56 Validation	42
3.2	TASOPT Validation	43
3.3	NPSS GE90 Validation	46

4	Optimum-Aircraft Parametric Studies	49
4.1	Optimum-Aircraft Sensitivity to Specified Mission Range	50
4.2	Optimum-Aircraft Sensitivity to Specified Minimum Climb Rate . . .	51
4.3	Full Mission Versus Cruise Only Optimization	53
4.4	Multi-Mission Optimization	54
4.5	Sensitivity Discussion	56
5	Conclusion	59
A	Diffuser, Fan, and Compressor Model	61
B	Turbine Model	63
C	Flight Profile and Aircraft Sizing Model	65
C.1	Weight Breakdown	67
C.2	Aircraft Sizing	68
C.3	General Aircraft Performance	69
C.4	Climb	71
C.5	Cruise	72
C.6	Atmosphere Model	72
D	Signomial Equality Constraint Intuition	75
E	Engine Boundary Layer Ingestion	77

List of Figures

1-1	Engine model architecture.	21
1-2	The non-convex signomial inequality drag constraint $C_D \geq f(C_L)$ and GP approximations about two different points.	24
1-3	The signomial equality constraint $C_D = f(C_L)$ and its approximation.	25
2-1	TASOPT engine station numbering, which was adopted for this thesis.	27
2-2	E3 fan map with an estimated engine operating line in red. The map's design pressure ratio is 1.7.	36
2-3	E3 compressor map with an estimated engine operating line in red. The map's design pressure ratio is 26.	37
2-4	Monomial approximations to the E3 compressor map spine.	38
2-5	Monomial approximations to the E3 fan map spine.	38
4-1	Total fuel burn versus mission range.	50
4-2	Initial engine thrust, core and fan thrust, climb and cruise TSFC, as well as engine weight for a variety of mission ranges.	51
4-3	Initial fan and core thrust versus minimum initial climb rate.	52
4-4	Engine weight versus minimum initial climb rate.	53
4-5	Fan inlet area (A_2) versus minimum initial climb rate.	54
4-6	Initial climb and cruise TSFC versus minimum initial climb rate.	55
4-7	Sensitivity to fan design pressure ratio versus minimum initial climb rate.	58

C-1	Xfoil NC130 airfoil drag data (dots) and a posynomial approximation of the data (solid line) for a Reynolds number of 20 million.	70
E-1	Cartoon illustrating boundary layer growth on a BLI equipped aircraft similar to the D8.	77

List of Tables

2.1	Assumed gas properties for each engine component	28
3.1	Input values used in all three validation cases.	42
3.2	The number of GP solves and solution time for each validation case. .	42
3.3	Input values used for CFM56 engine validation.	43
3.4	The two operating points used during CFM56 validation.	43
3.5	NPSS CFM56 validation results, expected to be similar when $h_f = 40.8$ MJ/kg.	44
3.6	The three operating points used when validating the presented model against TASOPT.	45
3.7	Input values used for TASOPT engine validation.	45
3.8	TASOPT validation results with engine weight capped at 110% of the TASOPT value, expected to be similar at on design.	45
3.9	The two operating points used when validating the presented model against the GE90 like NPSS model.	46
3.10	Input values used for GE90 engine validation	46
3.11	NPSS GE90 validation results, expected to be similar at both operating points.	47
4.1	Aircraft sizing and flight profile inputs.	50
4.2	Differences in engine size when accounting for the full mission profile and just cruise.	54
4.3	Differences in engine size for the presented multi-mission optimization formulation and a single 2,000 nm range mission optimization.	56

4.4 Top engine design value sensitivities in the aircraft optimization example for a single 2,000 nm mission. 57

4.5 Top aircraft design and mission parameter sensitivities in the aircraft optimization example. 57

Nomenclature

a = speed of sound

α = engine by-pass ratio

A = flow area

c_k = constant in a monomial, posynomial, or signomial

C_D = aircraft drag coefficient

C_L = aircraft lift coefficient

C_p = working fluid constant pressure specific heat

D = drag force

η = efficiency

F = total engine thrust

f_c = cooling flow by-pass ratio ($\dot{m}_{\text{cool}}/\dot{m}_{\text{core}}$)

f_f = fuel/air ratio

\bar{f}_o = one minus the percent of core mass flow bled for pressurization, electrical generation, etc.

F_6 = core engine thrust

F_8 = fan engine thrust

F_{sp} = overall specific thrust

γ = ratio of working fluid specific heats

G_f = fan gearing ratio

h, h_t = static and stagnation enthalpy

h_f = fuel heat of combustion

M_{engine} = engine mass

N_f = normalized fan spool speed

N_1 = normalized LPC spool speed

N_2 = normalized HPC spool speed
 \dot{m} = mass flow
 \bar{m} = corrected mass flow
 M = Mach number
 $m(u)$ = monomial function of u
 P, P_t = static and stagnation pressure
 $\pi(\cdot)$ = pressure ratio across component (\cdot)
 $p(u)$ = posynomial function of u
 R = specific gas constant
 ρ = air density
 r_{uc} = cooling flow velocity ratio
 $s(u)$ = signomial function of u
 T, T_t = static and stagnation temperature
 TSFC = thrust specific fuel consumption
 \mathbf{u} = vector of all decision variables
 u = flow velocity
 V = aircraft velocity
 W_{engine} = engine weight
 Z = total/static temperature ratio
 $(\cdot)_b$ = combustor quantity
 $(\cdot)_{\text{cool}}$ = cooling flow quantity
 $(\cdot)_{\text{core}}$ = core stream quantity
 $(\cdot)_d$ = diffuser quantity
 $(\cdot)_{\dots D}$ = nominal design point quantity
 $(\cdot)_f$ = fan quantity
 $(\cdot)_{\text{fan}}$ = fan stream quantity
 $(\cdot)_{\text{fn}}$ = fan nozzle quantity
 $(\cdot)_{\text{HP}}$ = high pressure shaft quantity
 $(\cdot)_{\text{HPC}}$ = high pressure compressor quantity
 $(\cdot)_{\dots i}$ = quantity at engine station i

$(\cdot)_{LP}$ = low pressure shaft quantity

$(\cdot)_{LPC}$ = low pressure compressor quantity

$(\cdot)_{SL}$ = sea level quantity

$(\cdot)_t$ = stagnation quantity

$(\cdot)_{total}$ = fan and core stream quantity

$(\cdot)_{+1}$ = (\cdot) plus one

Acronyms

BLI = boundary layer ingestion

BPR = by-pass ratio

FPR = fan pressure ratio

GP = geometric program

HP = high pressure

HPC = high pressure compressor

HPT = high pressure turbine

LP = low pressure

LPC = low pressure compressor

LPT = low pressure turbine

NLP = nonlinear program

NPSS = Numerical Propulsion System Simulation

OPR = overall pressure ratio

SP = signomial program

TASOPT = Transport Aircraft System OPTimization

TOC = top of climb

Chapter 1

Introduction

A key goal of conceptual aircraft design is to quantify basic trade offs between competing mission requirements and between the various aircraft sub-systems. For an exhaustive study, multiple design parameter sweeps must be performed, ideally with an optimum conceptual aircraft produced for each point examined. Because typical aircraft design-parameter spaces are quite large, such trade studies demand a reliable and efficient system-level optimization method. As noted by Martins[21], there exists a need for new multidisciplinary design optimization (MDO) tools that exhibit fast convergence for medium and large scale problems. In pursuit of this goal, Hoburg et al.[15] and Kirschen et al.[19] have proposed formulating aircraft conceptual design models as geometric programs (GP) or signomial programs (SP). Geometric and signomial programs enable optimization problems with thousands of design variables to be reliably solved on laptop computers in a matter of seconds.

Such speed and reliability is possible because these formulations can be solved via convex optimization (in the case of GP), or via sequential convex optimization (in the case of SP). One limitation of GP methods is that all physical model equations must be posed as either posynomial inequality constraints or monomial equality constraints, which at first seems far too restrictive. One objective of this thesis is to show that this is not necessarily the case, and that even quite complex physical models can be recast into the necessary forms. This is accomplished in two ways. First, many, but not all, expressions that arise in turbofan design are directly compatible with

GP or can be closely approximated by posynomial constraints. Second, relationships that are not directly GP-compatible are often SP-compatible. SP is a non-convex extension of GP that can be solved locally as a sequence of GPs. While SPs sacrifice guarantees of global optimality, they can be solved far more reliably than general nonlinear programs (NLPs).

The specific example considered is the turbofan model in the Transport Aircraft System OPTimization (TASOPT)[10] conceptual design tool, which uses traditional optimization techniques. This model is a full 1D core+fan flowpath simulation based on first principles, which here will be recast into an SP-compatible form. This enables the construction of SP-compatible aircraft conceptual design models that address the complex design tradeoffs between engine and airframe parameters by treating the parameters as design variables. Such methods can produce much more realistic and higher-fidelity conceptual designs as starting points for subsequent preliminary and detailed design, with more reliability and much less time than would be required by the alternative MDO methods that combine traditional engine and airframe modules.

The SP-compatible engine model developed here is compared against TASOPT and two Georgia Tech Numerical Propulsion System Simulation (NPSS)[17] models to demonstrate that it produces the correct results. To demonstrate its effectiveness for SP aircraft optimization, the model is integrated into a simple commercial transport aircraft sizing optimization problem. Example aircraft parametric studies are presented, including a 2,460 variable multi-mission optimization problem that solves in 28 seconds.

1.1 Optimization Formulation

1.1.1 Model Architecture

The presented engine model is formulated as a single multi-point optimization problem with no engine on/off design point distinctions. All constraints are applied at every point in the flight, and the model selects the engine which most optimally meets

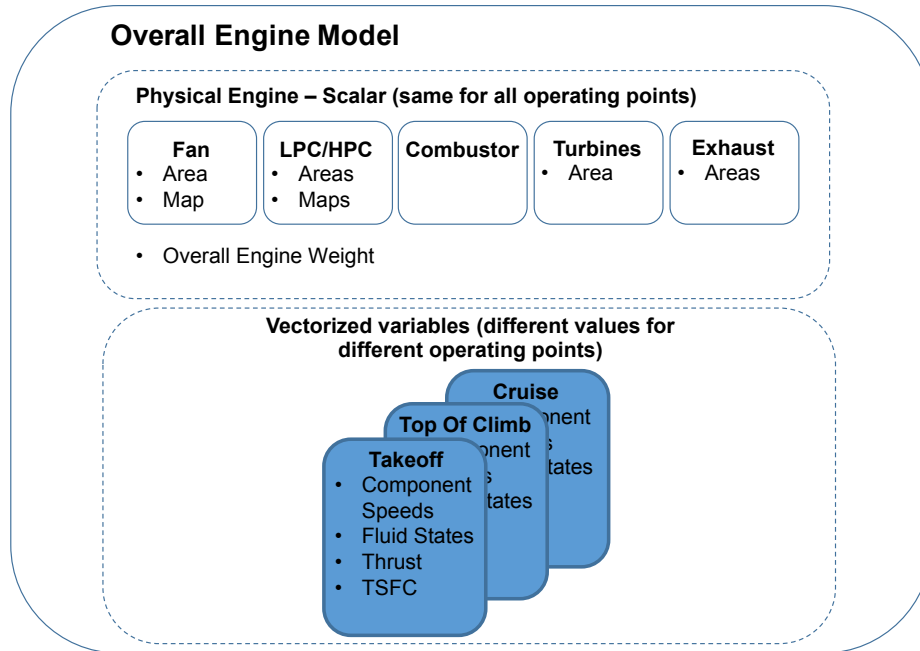


Figure 1-1: Engine model architecture.

all constraints. This, coupled with the fact SPs are solved all at once (i.e. there is no order of operations), greatly simplifies integrating the engine into a full aircraft system model. Figure 1-1 illustrates the engine model’s overall architecture. It is worth noting no initial guesses are supplied to the presented model.

1.1.2 Solution Method

The models in this thesis consist of sets of constraints that are compatible with SP. All SPs presented in this thesis were solved on a laptop computer using a combination of GPkit[7] and MOSEK[4]. GPkit, developed at MIT, is a python package that enables the fast and intuitive formulation of geometric (GP) and signomial programs. GPkit has a built in heuristic for solving SPs as a series of GP approximations. GPkit binds with open source and commercial interior point solvers to solve individual GPs. GPkit source code is available at <https://github.com/hoburg/gpkit> and the turbofan engine model is available at <https://github.com/hoburg/turbofan>.

1.1.3 Geometric Programming

Introduced in 1967 by Duffin et al. [12], a geometric program (GP) is a type of constrained optimization problem that becomes convex after a logarithmic change of variables. Modern interior point methods allow a typical sparse GP with tens of thousands of decision variables and tens of thousands of constraints to be solved in minutes on a desktop computer [6]. These solvers do not require an initial guess and guarantee convergence to a *global* optimum, assuming a feasible solution exists. If a feasible solution does not exist, the solver will return a certificate of infeasibility. These impressive properties are possible because a GP's objective and constraints consist of only monomial and posynomial functions, which can be transformed into convex functions in log space.

A monomial is a function of the form

$$m(\mathbf{u}) = c \prod_{j=1}^n u_j^{a_j} \quad (1.1)$$

where $a_j \in \mathbb{R}$, $c \in \mathbb{R}_{++}$ and $u_j \in \mathbb{R}_{++}$. An example of a monomial is the common expression for lift, $\frac{1}{2}\rho V^2 C_L S$. In this case, $\mathbf{u} = (\rho, V, C_L, S)$, $c = 1/2$, and $a = (1, 2, 1, 1)$.

A posynomial is a function of the form

$$p(\mathbf{u}) = \sum_{k=1}^K c_k \prod_{j=1}^n u_j^{a_{jk}} \quad (1.2)$$

where $a_{jk} \in \mathbb{R}$, $c_k \in \mathbb{R}_{++}$ and $u_j \in \mathbb{R}_{++}$. A posynomial is a sum of monomials. Therefore, all monomials are also one-term posynomials.

A GP minimizes a posynomial objective function subject to monomial equality and posynomial inequality constraints. A GP written in standard form is

$$\begin{aligned} & \text{minimize } p_0(\mathbf{u}) \\ & \text{subject to } p_i(\mathbf{u}) \leq 1, i = 1, \dots, n_p, \\ & m_i(\mathbf{u}) = 1, i = 1, \dots, n_m \end{aligned} \quad (1.3)$$

where p_i are posynomial functions, m_i are monomial functions, and $\mathbf{u} \in \mathbb{R}_{++}^n$ are the decision variables. Once a problem has been formulated in the standard form (Equation 1.3), it can be solved efficiently.

1.1.4 Signomial Programming

It is not always possible to formulate a design problem as a GP. This motivates the introduction of signomials. Signomials have the same form as posynomials

$$s(\mathbf{u}) = \sum_{k=1}^K c_k \prod_{j=1}^n u_j^{a_{jk}} \quad (1.4)$$

but the coefficients, $c_k \in \mathbb{R}$, can now be any (including non-positive) real numbers.

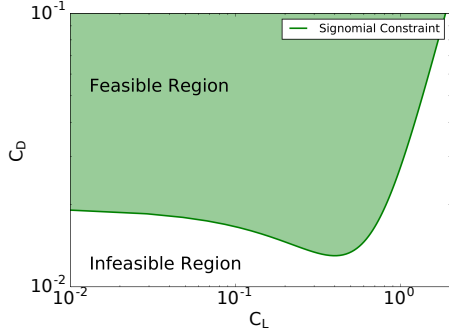
A signomial program (SP) is a generalization of GP where the inequality constraints can be composed of signomial constraints of the form $s(u) \leq 0$. The log transform of an SP is not a convex optimization problem, but it is a difference of convex optimization problem that can be written in log-space as

$$\begin{aligned} & \text{minimize } f_0(\mathbf{x}) \\ & \text{subject to } f_i(\mathbf{x}) - g_i(\mathbf{x}) \leq 0, i = 1, \dots, m \end{aligned} \quad (1.5)$$

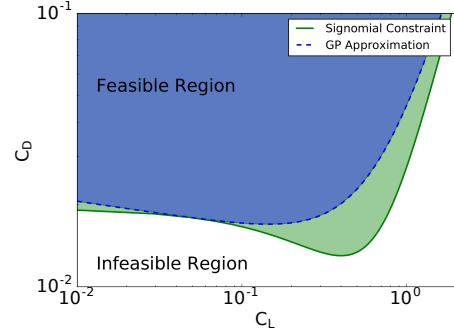
where f_i and g_i are convex.

There are multiple algorithms that reliably solve signomial programs to *local* optima [5, 20]. This is done by solving a sequence of GPs, where each GP is a local approximation to the SP, until convergence occurs. It is worth noting that the introduction of even a single signomial constraint to any GP turns the GP into a SP, thus losing the guarantee of solution convergence to a global optimum. A favorable property of SP inequalities is that the feasible set of the convex approximation is always a subset of the original SP's feasible set, as depicted in Figure 1-2. This removes the need for trust regions and makes solving SPs substantially more reliable than solving general nonlinear programs.

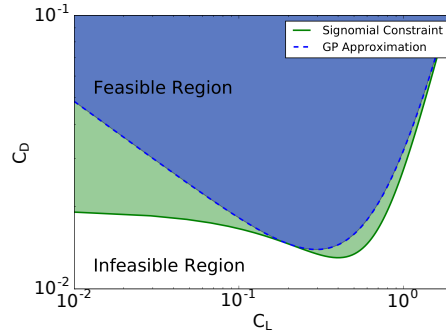
The previously presented difference of convex technique works only for signomial



(a) Signomial inequality drag constraint.



(b) Convex approximation about $C_L = 0.05$.



(c) Convex approximation about $C_L = 0.20$.

Figure 1-2: The non-convex signomial inequality drag constraint $C_D \geq f(C_L)$ and GP approximations about two different points.

inequality, posynomial inequality, and monomial equality or inequality constraints. Signomial equality constraints can be approximated by monomials, as shown in Figure 1-3. Signomial equalities are the least desirable type of constraint due to the approximations involved. This work contains five signomial equality constraints. For additional details on how signomial equalities are approximated, see Opgenoord et al.[24]. For intuition on when signomial equality constraints are required, see Appendix D.

1.2 Terminology

Before proceeding, it is useful to introduce some of the vocabulary used to describe this work.

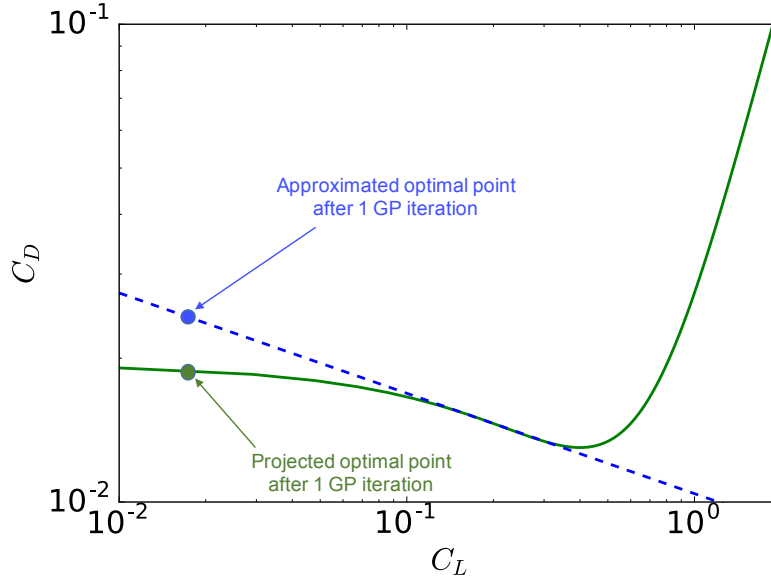


Figure 1-3: The signomial equality constraint $C_D = f(C_L)$ and its approximation.

1.2.1 Models

A model is a set of GP and/or SP compatible constraints. The input to a model is the value of any fixed variables or constants appearing the model. Two models that share variables may be linked by concatenating their constraints.

1.2.2 GP- and SP-compatibility

A constraint is GP-compatible if it can be written as either a monomial equality (Equation 1.1) or a posynomial inequality (Equation 1.2). A model is GP-compatible if its objective is a monomial or posynomial and all its constraints are GP compatible. A constraint is SP-compatible if it can be written as a signomial inequality (Equation 1.4) or equality. A model is SP-compatible if its objective is a monomial, posynomial, or ratio of posynomials and all its constraints can be written as either monomial equalities, posynomial inequalities, signomial inequalities, or signomial equalities.

1.2.3 Static and Performance Models

The presented model is a multi-point optimization problem. To formulate the multi-point problem, two models are created for each engine component - a static and a performance model. The static model contains all variables and constraints that do not change between operating points, such as engine weight and nozzle areas. Performance models contain all constraints and variables that do change between operating points. For example, all constraints involving fluid states are contained in performance models. To simulate multiple engine operating points, the performance models are vectorized. When a model is vectorized, all the variables it contains become vectors, with each element corresponding to a different engine operating point. Figure 1-1 provides a visual representation of static and performance models.

Chapter 2

Model Derivation

Constraint derivation follows the general framework of the TASOPT turbofan model[10], with minor changes to facilitate the removal on the on-design/off-design distinction. TASOPT station numbering was adopted and is presented in Figure 2-1. The model assumes a two spool engine with two compressors and two turbines. The model can support a geared fan. Values of C_p and γ are assumed for each engine component and presented in Table 2.1. Isentropic relations were used to model working fluid state changes across turbomachinery components and a shaft power balance was enforced on both the low and high pressure shafts. Details of these models are discussed in Appendices A and B. Remaining submodels are described in the following sub-sections.

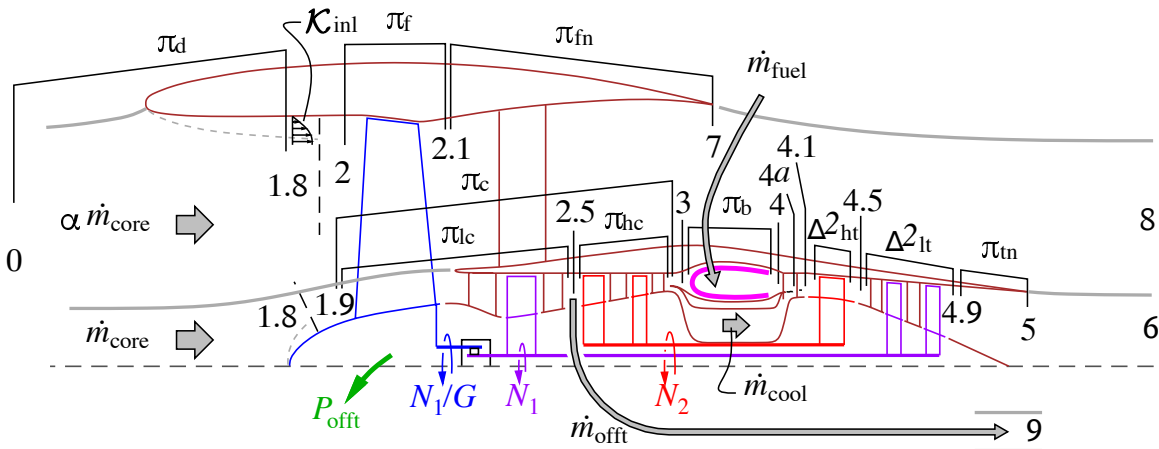


Figure 2-1: TASOPT engine station numbering, which was adopted for this thesis.

Table 2.1: Assumed gas properties for each engine component

Engine Component	C_p [J/kg/K]	γ	Corresponding Air Temperature [K]
Diffuser	1005	1.4	260
LPC	1008	1.398	350
HPC	1099	1.354	800
Combustor	1216	1.313	1500
HPT	1190	1.318	1300
LPT	1142	1.335	1000
Core Exhaust	1029	1.387	500
Fan Exhaust	1005	1.4	273

2.1 Combustor and Cooling Flow Mixing Model

The combustor and cooling flow constraints serve two purposes - to determine the fuel mass flow percentage and to account for the total pressure loss resulting from the mixing of the cooling flow and the working fluid in the main flow path. The flow mixing model is taken directly from TASOPT[10].

The fuel mass flow and T_{t_4} are constrained via an enthalpy balance (Equation 2.1) while Equations 2.2 and 2.3 determine the remaining station 4 states. η_b is the burner efficiency, a value less than one indicates a portion of injected fuel is not burned. The specified f_c is the cooling flow bypass ratio whose typical values range from 0.2-0.3, with lower values indicating a higher engine technology level. $C_{p_{fuel}}$ and h_f are taken as constants equal to 2010 J/kg/K and 43.003 MJ/kg respectively. T_{t_f} is the fuel's temperature when injected into the combustor and π_b is the combustor pressure ratio. Both are user inputs.

$$\eta_b f_f h_f \geq (1 - f_c)(h_{t_4} - h_{t_3}) + C_{p_{fuel}} f_f (T_{t_4} - T_{t_f}) \quad (2.1)$$

$$h_{t_4} = C_{p_c} T_{t_4} \quad (2.2)$$

$$P_{t_4} = \pi_b P_{t_3} \quad (2.3)$$

It is assumed the cooling flow is unregulated and engine pressure ratios are relatively constant so f_c will not change between operating points. Further, it is assumed the cooling flow is discharged entirely over the first row of inlet guide vanes (station 4a) and mixes completely with the main flow before the first row of turbine blades (station 4.1). The first row of inlet guide vanes requires the majority of the cooling flow, justifying this assumption.

The mixed out flow temperature at station 4.1 is computed with the enthalpy balance in Equation 2.4. Note this is a signomial equality.

$$h_{t_{4.1}} f_{f+1} = (1 - f_c + f_f) h_{t_4} + f_c h_{t_3} \quad (2.4)$$

The mixed-out state at station 4.1 is computed in terms of the temperature ratio Z_{4a} , which is introduced for GP compatibility.

$$Z_{4a} = 1 + \frac{1}{2}(\gamma - 1)(M_{4a})^2 \quad (2.5)$$

$$P_{4a} = P_{t_4} (Z_{4a})^{-\frac{\gamma_i}{\gamma_i - 1}} \quad (2.6)$$

$$u_{4a} = M_{4a} \sqrt{\gamma_{4a} R T_{t_4} / Z_{4a}} \quad (2.7)$$

Cooling flow velocity, u_{cool} , is defined by the user input cooling flow velocity ratio r_{uc} .

$$u_{cool} = r_{uc} u_{4a} \quad (2.8)$$

Static pressure rise during mixing is neglected and the station 4.1 state is computed

using stagnation relations. Equation 2.10 is a signomial equality constraint.

$$P_{t_{4.1}} = P_{4a} \left(\frac{T_{t_{4.1}}}{T_{4.1}} \right)^{\frac{\gamma_i}{\gamma_i - 1}} \quad (2.9)$$

$$T_{4.1} = T_{t_{4.1}} - \frac{1}{2} \frac{u_{4.1}^2}{C_{pc}} \quad (2.10)$$

Rather than introduce a full momentum balance, this model approximates $u_{4.1}$ as the geometric average of core and cooling flow velocities.

$$f_{f+1} u_{4.1} = \sqrt{f_{f+1} u_{4a} \alpha_{cool} u_{cool}} \quad (2.11)$$

2.2 Area, Mass Flow, and Speed Constraints

Either the engine's thrust or the turbine inlet temperature must be constrained via Equation 2.12 or 2.13. In a full aircraft optimization problem, F_{spec} can be linked to thrust requirements in an aircraft performance model. When the engine model is run in isolation, F_{spec} or $T_{t_{4.1}}$ must be specified by the user.

$$F = F_{spec} \quad (2.12)$$

$$T_{t_{4.1}} = T_{t_{4spec}} \quad (2.13)$$

Component speed ratios are determined by the turbo-machinery maps (Section 2.3). Only the ratio of component speed to the component's nominal design speed is considered, so the nominal design speed is arbitrarily set to one. Thus, an LPC speed of $N_1 = 1.1$ should be thought of as an LPC speed 10 percent faster than the components nominal design speed, not a value 10 percent over max RPM. This model does not attempt to constrain actual RPM values.

The fan and LPC both lie on the low pressure shaft so their speeds are correlated via Equation 2.14, which allows for a user selected gearing ratio G_f . Additionally,

a maximum allowable speed is set for the fan and compressors. The max speed of 1.1 is estimated from TASOPT output. If an upper bound is not placed on speed, the optimizer will indefinitely increase component speed to drive OPR higher. When solving across an engine mission profile, the upper speed bound will only be achieved at the engine's most demanding operating point.

$$N_f = G_f N_1 \quad (2.14)$$

$$N_1 \leq 1.1 \quad (2.15)$$

$$N_2 \leq 1.1 \quad (2.16)$$

Constraints on the mass flux through engine components are used to ensure each engine operating point corresponds to an engine of the same physical size. The station 5 and 7 exit states are determined using user specified nozzle pressure ratios as well as isentropic and stagnation relations.

$$P_{t_5} = \pi_{tn} P_{t_{4.9}} \quad (2.17)$$

$$P_{t_7} = \pi_{fn} P_{t_2} \quad (2.18)$$

$$P_i \geq P_0 \quad (2.19)$$

$$\frac{P_i}{P_{t_i}} = \left(\frac{T_i}{T_{t_i}} \right)^{\frac{\gamma}{\gamma-1}} \quad (2.20)$$

$$\left(\frac{T_i}{T_{t_i}} \right)^{-1} \geq 1 + 0.2(M_i)^2 \quad (2.21)$$

Equation 2.22 is a deviation from constraints in traditional engine models that

use Newton’s method or a comparable iterative procedure. In many methods, M_5 and M_7 are set equal to 1 if M_6 or M_8 is respectively greater than 1 so that the exit nozzle is choked. If M_6 or M_8 is less than 1, then M_5 and M_7 are constrained to be less than 1. A switch is used to change constraints mid solve. It is not possible to switch constraints during a GP solve. Therefore, M_5 and M_7 are constrained to be less than or equal to 1, regardless of M_6 and M_8 . For the mild choking typical in efficient turbofans, the effects of this reformulation are negligible, as confirmed by Section 3.

$$M_i \leq 1 \tag{2.22}$$

Equations 2.23 to 2.33 set A_2 , $A_{2.5}$, A_5 , and A_7 . Note $M_{2.5}$ is set by the user and M_2 is either linked to an aircraft performance model or set by the user.

$$a_i = \sqrt{\gamma RT_i} \tag{2.23}$$

$$u_i = a_i M_i \tag{2.24}$$

$$\rho_i = \frac{P_i}{RT_i} \tag{2.25}$$

In the static property calculations, the temperature ratio Z_i is again introduced for GP compatibility.

$$Z_i = 1 + \frac{\gamma_i - 1}{2} M_i^2 \tag{2.26}$$

$$P_i = P_{t_i} (Z_i)^{\frac{\gamma}{1-\gamma}} \tag{2.27}$$

$$T_i = T_{t_i} Z_i^{-1} \tag{2.28}$$

$$h_i = C_{p_i} T_i \quad (2.29)$$

In equation 2.30, the value of $C_{p_i} - R$ is precomputed and substituted into the constraint to make it GP compatible.

$$u_i = M_i \sqrt{C_{p_i} R T_i / (C_{p_i} - R)} \quad (2.30)$$

$$\dot{m}_{\text{fan}} = \rho_7 A_7 u_7 \quad (2.31)$$

$$\dot{m}_{\text{core}} \bar{f}_o = \rho_5 A_5 u_5 / f_{f+1} \quad (2.32)$$

$$\alpha = \dot{m}_{\text{fan}} / \dot{m}_{\text{core}} \quad (2.33)$$

Full turbine maps are not used to constrain turbine mass flow. Instead, it is assumed the entry to each turbine is always choked. This leads to two constraints, each setting the corrected mass flow at turbine entry equal to the estimated nominal value.

$$\bar{m}_{\text{HPT}_D} = \bar{m}_{\text{HPC}} f_{f+1} \bar{f}_o (P_{t_{2.5}} / P_{t_{4.1}}) \sqrt{T_{t_{4.1}} / T_{t_{2.5}}} \quad (2.34)$$

$$\bar{m}_{\text{LPT}_D} = \bar{m}_{\text{LPC}} f_{f+1} \bar{f}_o (P_{t_{1.8}} / P_{t_{4.5}}) \sqrt{T_{t_{4.5}} / T_{t_{1.8}}} \quad (2.35)$$

The optimized nominal core mass flow is computed via equation 2.36. \hat{T}_i and \hat{P}_i represent the estimated nominal state at engine station i . The values of \hat{T}_{t_4} , \hat{P}_{t_2} , and \hat{T}_{t_2} are set by the user while all other \hat{T} and \hat{P} values are estimated using the isentropic relations, component design pressure ratios, and a shaft power balance. This process is shown in equation set 2.37. Nominal mass flows are allowed to vary plus or minus 30 percent from their estimated values to account for uncertainty in the estimation process and ensure that if the nominal design condition is estimated

to occur at the aircraft's average altitude, the optimizer can place the nominal state anywhere in the flight. Optimization of the nominal state enables removal of the a priori specification of an engine on-design point.

$$\begin{aligned}\bar{m}_{\text{component}_D} &\leq 1.3 f_{f+1} \bar{f}_o \dot{m}_{\text{core}_D} \sqrt{\hat{T}_{t_i}/T_{\text{ref}}/(\hat{P}_{t_i}/P_{\text{ref}})} \\ \bar{m}_{\text{component}_D} &\geq 0.7 f_{f+1} m_{\text{off}} \dot{m}_{\text{core}_D} \sqrt{\hat{T}_{t_i}/T_{\text{ref}}/(\hat{P}_{t_i}/P_{\text{ref}})}\end{aligned}\quad (2.36)$$

$$\begin{aligned}\hat{P}_i &= \pi_{\text{component}} \hat{P}_{i-1} \\ \hat{T}_{t_i} &= \hat{T}_{t_{i-1}} (\pi_{\text{component}})^{\frac{\gamma-1}{\gamma \eta_i}} \\ \hat{T}_{t_{4.5}} &= \hat{T}_{t_{4.1}} - (\hat{T}_{t_3} - \hat{T}_{t_{2.5}}) \\ \hat{T}_{t_{4.9}} &= \hat{T}_{t_{4.5}} - (\hat{T}_{t_{2.5}} - \hat{T}_{t_{2.1}}) \\ \hat{\pi}_{\text{HPT}} &= \left(\frac{\hat{T}_{t_{4.5}}}{\hat{T}_{t_{4.1}}} \right)^{\frac{\eta_i \gamma}{\gamma-1}} \\ \hat{P}_{t_{4.5}} &= \hat{\pi}_{\text{HPT}} \hat{P}_{t_3}\end{aligned}\quad (2.37)$$

2.3 Fan and Compressor Maps

Fan and compressor maps are required to accurately constrain fan and compressor pressure ratios. Every engine has different compressor maps that result from detailed turbo-machinery design. The present model does not attempt to take into account factors causing variations in turbo-machinery maps. Instead, a simple compressor and fan map is assumed and applied to all engines. As argued in section 3, this is accurate enough for aircraft conceptual design optimization.

GP compatible fan and compressor maps were derived from NASA's Energy Efficient Engine (E3) program[13] turbomachinery maps, which are presented in Figures 2-2 and 2-3. These are also the maps used in TASOPT. Blue curves are lines of constant component speed and red curves are the estimated engine operating line, or

spine. Each spine can be parameterized as either $\pi = f(\bar{m})$ or $\pi = f(N)$, where \bar{m} is normalized corrected mass flow and N is component speed. The normalized corrected mass for for each components is defined below.

$$\bar{m}_{\text{HPC}} = \dot{m}_{\text{core}} \sqrt{T_{2.5}/T_{\text{ref}}}/(P_{t_{2.5}}/P_{\text{ref}}) \quad (2.38)$$

$$\bar{m}_{\text{LPC}} = \dot{m}_{\text{core}} \sqrt{T_2/T_{\text{ref}}}/(P_{t_2}/P_{\text{ref}}) \quad (2.39)$$

$$\bar{m}_{\text{fan}} = \dot{m}_{\text{fan}} \sqrt{T_2/T_{\text{ref}}}/(P_{t_2}/P_{\text{ref}}) \quad (2.40)$$

A GP compatible monomial approximation to the functions $\pi = f(\bar{m})$ and $\pi = f(N)$ was developed with GPfit[16, 18]. The approximations for both the compressor and fan map spine fits are given by Equations 2.41 through 2.44 and plotted in Figures 2-4 and 2-5.

$$\pi_{\text{comp}} = 20.1066(N)^{5.66} \quad (2.41)$$

$$\pi_{\text{comp}} = 25.049(\bar{m})^{1.22} \quad (2.42)$$

$$\pi_{\text{fan}} = 1.6289(N_f)^{0.871} \quad (2.43)$$

$$\pi_{\text{fan}} = 1.7908(\bar{m})^{1.37} \quad (2.44)$$

The fan map spine was only fit for speeds greater than 0.6. Single term fits are monomials that must pass through the origin, limiting their ability to capture fan trends for low speeds. During a typical flight, the low pressure spool speed (N_1) will rarely, if ever, drop below 0.6. The fitted map, combined with the constraint all pressure ratios are greater than 1, places an implicit lower bound on N_1 and N_f which may lead to modeling inaccuracy at low throttle settings. This is acceptable

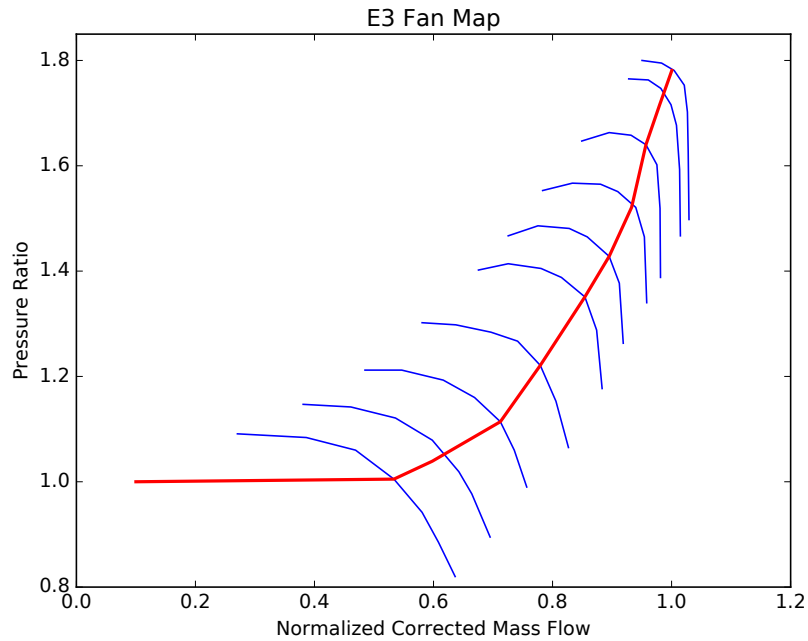


Figure 2-2: E3 fan map with an estimated engine operating line in red. The map's design pressure ratio is 1.7.

due to the proportionally small amount of fuel burned at low throttle settings. A two term polynomial fit yields a better approximation of the fan map, but was not used because it adds an additional signomial constraint.

Equations 2.45 through 2.47 are fan and compressor map approximations obtained by scaling the E3 map fits to an arbitrary design pressure ratio and constraining the pressure ratio be within 10 percent of the spine mass flow fit. This allows the operating point to move off the operating line while ensuring the operating point does not move into either the stall or surge regime. The user must specify at a minimum either fan, LPC, and HPC design pressure ratios or a maximum turbine inlet temperature ($T_{t4,1}$). The user may specify all four values. Setting fan, LPC, and HPC design pressure ratios values scales the maps and is distinct from specifying a full engine on-design operating point. If component design pressure ratios are left free, a maximum turbine inlet temperature must be specified so the cooling model prevents OPR from being driven to infinity.

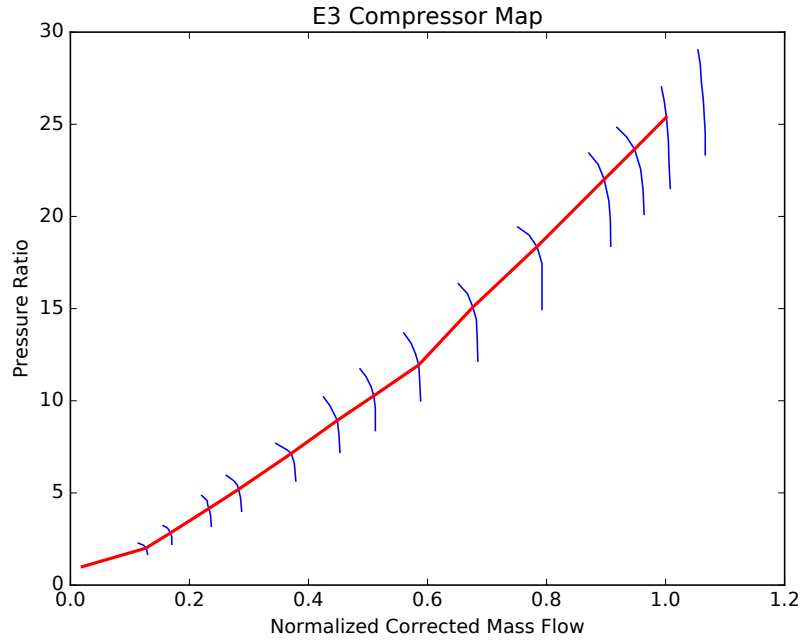
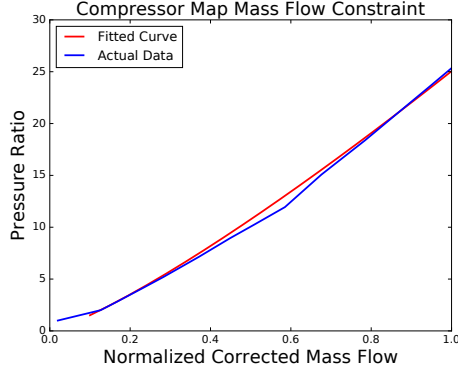


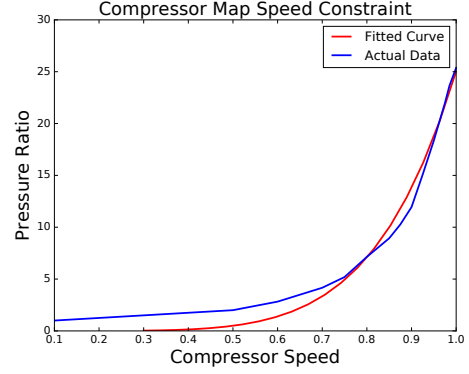
Figure 2-3: E3 compressor map with an estimated engine operating line in red. The map's design pressure ratio is 26.

$$\begin{aligned}
 \pi_{\text{fan}}\left(\frac{1.7}{\pi_{f_D}}\right) &= 1.6289(N_f)^{0.871} \\
 \pi_{\text{fan}}\left(\frac{1.7}{\pi_{f_D}}\right) &\geq (0.9)1.7908(\bar{m}_f)^{1.37} \\
 \pi_{\text{fan}}\left(\frac{1.7}{\pi_{f_D}}\right) &\leq (1.1)1.7908(\bar{m}_f)^{1.37}
 \end{aligned} \tag{2.45}$$

$$\begin{aligned}
 \pi_{\text{LPC}}\left(\frac{26}{\pi_{\text{LPC}_D}}\right) &= 20.1066(N_1)^{5.66} \\
 \pi_{\text{LPC}}\left(\frac{26}{\pi_{\text{rmLPC}_D}}\right) &\geq (0.9)25.049(\bar{m}_{\text{LPC}})^{1.22} \\
 \pi_{\text{LPC}}\left(\frac{26}{\pi_{\text{rmLPC}_D}}\right) &\leq (1.1)25.049(\bar{m}_{\text{LPC}})^{1.22}
 \end{aligned} \tag{2.46}$$

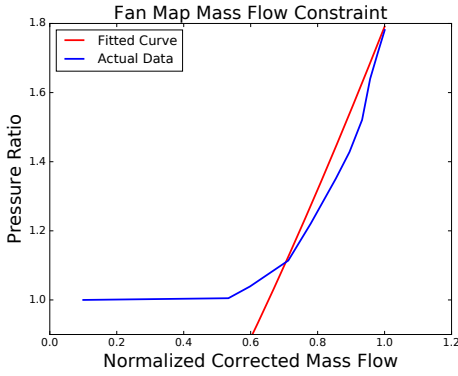


(a) Mass flow parametrization

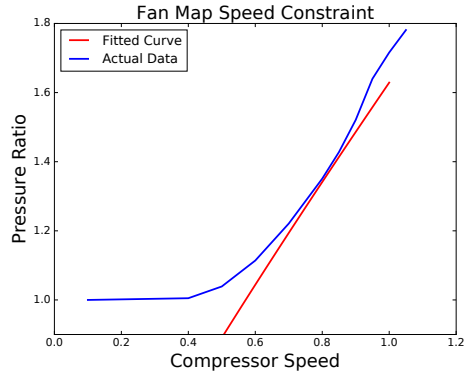


(b) Speed parametrization

Figure 2-4: Monomial approximations to the E3 compressor map spine.



(a) Mass flow parametrization



(b) Speed parametrization

Figure 2-5: Monomial approximations to the E3 fan map spine.

$$\begin{aligned}
 \pi_{\text{HPC}} \left(\frac{26}{\pi_{\text{HPC}_D}} \right) &= 20.1066(N_2)^{5.66} \\
 \pi_{\text{HPC}} \left(\frac{26}{\pi_{\text{HPC}_D}} \right) &\geq (0.9)25.049(\bar{m}_{\text{HPC}})^{1.22} \\
 \pi_{\text{HPC}} \left(\frac{26}{\pi_{\text{HPC}_D}} \right) &\leq (1.1)25.049(\bar{m}_{\text{HPC}})^{1.22}
 \end{aligned} \tag{2.47}$$

It is possible to fit a full compressor map instead of just the spine. However, there is no way to distinguish valid map points from points in the surge/stall regime. The optimizer will push the operating point towards these sections of the map, resulting in a physically invalid solution.

2.4 Exhaust State Model

Thrust is determined with a momentum balance. Station 6 (core exhaust) and 8 (fan exhaust) velocities are computed by equations 2.48 to 2.52 which employ the stagnation relations and assume isentropic flow expansion.

$$\left(\frac{P_i}{P_{t_i}}\right)^{\frac{\gamma_i-1}{\gamma_i}} = \frac{T_i}{T_{t_i}} \quad (2.48)$$

$$P_i = P_0 \quad (2.49)$$

$$h_{t_i} = C_{p_i} T_{t_i} \quad (2.50)$$

$$h_i = C_{p_i} T_i \quad (2.51)$$

$$u_i^2 + 2h_i \leq 2h_{t_i} \quad (2.52)$$

Fan and core thrust (F_8 and F_6) are computed with a momentum balance and summed to set the total thrust.

$$F_8/(\alpha\dot{m}_{\text{core}}) + u_0 \leq u_8 \quad (2.53)$$

$$F_6/(\bar{f}_o\dot{m}_{\text{core}}) + u_0 \leq u_6 \quad (2.54)$$

$$F \leq F_6 + F_8 \quad (2.55)$$

The specific thrust and corresponding thrust specific fuel consumption then follow.

$$F_{\text{sp}} = F/(a_0\alpha_{+1}\dot{m}_{\text{core}}) \quad (2.56)$$

$$\text{TSFC} = \frac{f_t g}{F_{\text{sp}} a_0 \alpha_{+1}} \quad (2.57)$$

2.5 Engine Weight

In an aircraft optimization problem there is a downward pressure on engine weight. Consequently, the TASOPT[10] engine weight model can be relaxed into a posynomial inequality constraint. The TASOPT engine weight model is a fit to production engine data and does not account for the weight of a gearbox in a geared turbofan. The GP compatible engine mass constraint, taken from TASOPT[10], is presented below. \dot{m}_{total} is defined by Equation 2.59.

$$M_{\text{engine}} \geq \frac{\dot{m}_{\text{total}}}{(100 \text{lbm/s}) \alpha_{+1}} \left(1684.5 \text{ lbm} + 17.7 \text{ lbm} \frac{\pi_f \pi_{\text{LPC}} \pi_{\text{HPC}}}{30} + 1662.2 \text{ lbm} \left(\frac{\alpha}{5} \right)^{1.2} \right) \quad (2.58)$$

\dot{m}_{core} is written in the equivalent form $\dot{m}_{\text{total}}/(\alpha_{+1})$ so an increase in either core or fan mass flow corresponds to an increase in engine weight, placing required downward pressure on both mass flows.

$$\dot{m}_{\text{total}} \geq \dot{m}_{\text{core}} + \dot{m}_{\text{fan}} \quad (2.59)$$

Chapter 3

Model Validation

The presented model was validated against the output of a CFM56-7B27 like NPSS model, a GE90-94B like NPSS model, and TASOPT. The NPSS models were developed by Georgia Tech with publicly available data under the FAA’s Environmental Design Space effort[22]. The NPSS output was provided by NASA. The TASOPT data was taken from a 737-800 optimization run. The TASOPT engine output should mirror that of Georgia Tech’s CFM56 like model because the CFM56-7B family powers all 737 Next Gen aircraft[1]. The intent of the validation studies was to verify the model’s physics modeling, not to find the most optimal engine. Essentially, during validation the model was used for engine analysis instead of optimization.

In all validation cases, BPR was constrained to be less than the validation data’s max BPR. This prevents BPR from growing without bound. During validation, the objective function was the sum of all climb TSFCs plus ten times the cruise TSFC. Cruise TSFC was weighted by a factor of ten to capture the fact that a commercial aircraft spends the majority of each flight in cruise. Optimizing TSFC does not apply a downward pressure to engine weight. Thus, engine weight was capped at the simulated engine’s predicted/actual engine weight.

$$\text{objective} = \sum \text{TSFC}_{\text{climb}} + 10\text{TSFC}_{\text{cruise}} \quad (3.1)$$

Component polytropic efficiencies, duct pressure losses, cooling flow bypass ratio,

Table 3.1: Input values used in all three validation cases.

Variable	Value	Units
T_{t_f}	435	K
$C_{p_{4.1}}$	1.280	KJ/kg/K
$C_{p_{4.5}}$	1.184	KJ/kg/K

Table 3.2: The number of GP solves and solution time for each validation case.

Validation Case	Number of GP solves	Solution Time [s]
CFM56	9	5.73
TASOPT	6	3.31
GE90	10	4.34

and max BPR are estimated from TASOPT/NPSS output. To mitigate errors due to the SP model’s assumed gas properties, TASOPT computed turbine C_p values were used in all three validation cases (NPSS computed C_p was not available in the provided output). These values, along with the assumed fuel temperature, are presented in Table 3.1.

Validation solution speeds are presented in Table 3.2.

3.1 NPSS CFM56 Validation

The SP model’s input values are given in Table 3.3. The SP model was constrained by two operating points, on-design and TOC, detailed in Table 3.4. The cruise and TOC operating points have similar ambient conditions and thrust requirements. The SP model should place the on-design point near the NPSS on-design point, producing little variation in predicted TSFC. Validation results are given in Table 3.5.

The SP turbofan model was solved for two different h_f values. Typically, the SP model has an h_f of 43.003 MJ/kg. However, Georgia Tech’s NPSS model has an implied h_f value of 40.8 MJ/kg, 5.12 percent less than SP model’s value and 2

Table 3.3: Input values used for CFM56 engine validation.

Variable	Value	Variable	Value
π_{fD}	1.685	α_{\max}	5.105
π_{LPCD}	1.935	f_c	0.19036
π_{HPCD}	9.369	η_{fan}	0.9005
η_b	0.9827	η_{LPC}	0.9306
G_f	1	η_{HPC}	0.9030
\bar{f}_o	0.9556	η_{HPT}	0.9030
η_{LPT}	0.8851	η_{HP}, η_{LP}	0.97
π_{tn}	0.98	π_b	0.94
π_d	0.98	π_{fn}	0.98
W_{engine}	23,201 N		

Table 3.4: The two operating points used during CFM56 validation.

Flight Condition	Altitude [ft]	Mach Number	Thrust [lbf]
TOC	35,000	0.8	5,961.9
On-Design (cruise)	35,000	0.8	5,496.4

MJ/kg below the minimum h_f of Jet A[23]. Solving the SP model with an h_f of 40.8 MJ/kg reduces the percent error at each operating point by approximately 5 percent. The remaining error can be accounted for by variations in component maps and gas properties.

3.2 TASOPT Validation

The SP turbofan model was validated against three TASOPT operating points: take-off, TOC, and on-design. The parameters for each operating point are given in Table 3.6. The constant input values are given in Table 3.7. Limiting the SP engine weight

Table 3.5: NPSS CFM56 validation results, expected to be similar when $h_f = 40.8$ MJ/kg.

Flight Condition	Predicted TSFC [1/hr]	NPSS TSFC [1/hr]	% Difference
On Design (SP $h_f = 43.003$ MJ/kg)	0.6335	0.6793	-6.74
On Design (SP $h_f = 40.8$ MJ/kg)	0.6679	0.6793	-1.68
Top of Climb (SP $h_f = 43.003$ MJ/kg)	0.6431	0.6941	-7.34
Top of Climb (SP $h_f = 40.8$ MJ/kg)	0.6780	0.6941	-2.31
TASOPT On-Design (implied $h_f = 42.68$ MJ/kg)	0.63403	0.6941	-6.66

to the TASOPT engine weight results in TSFC errors of 10.6 percent, 18.0 percent, and 7.9 percent at takeoff, TOC, and the on-design point (cruise) respectively. This error results from the engine weight constraint, Equation 2.58, as well as the fan and compressor maps (Section 2.3), which set the component pressure ratios, placing an implicit upper bound on engine mass flow. At the on-design point, the SP engine has a core mass flow 15.6 percent lower than the TASOPT engine. To match the TASOPT engine’s thrust, the SP engine must impart a larger velocity change to the working fluid; this increases TSFC. TASOPT[10] uses a different approximation to the E3 fan and compressor maps which allow its engines to achieve a greater mass flow for a given engine weight.

If the SP engine weight is instead capped at 110 percent of the TASOPT engine weight, the mass flow discrepancy is reduced to 0.1 percent. The TSFC errors for this case are presented in in Table 3.8. Note the on-design TSFC error is now less than one percent. No matter the cap on engine weight, the greatest TSFC error occurs at the TOC condition. At TOC, the low pressure spool is at its max allowed speed of 1.1. As discussed in section 2.3, the SP model’s fan map is conservative, particularly for high fan speeds. At a spool speed of 1.1 the SP model predicts a FPR of 1.75 while TASOPT has a FPR of 1.87, 6.28 percent higher. The SP model’s lower FPR causes the engine to produce more core thrust, lowering efficiency and increasing TSFC.

Table 3.6: The three operating points used when validating the presented model against TASOPT.

Flight Condition	Altitude [ft]	Mach Number	Thrust [lbf]
Take-Off	0	0.223	21,350
TOC	35,000	0.8	6,768
On-Design (cruise)	35,000	0.8	4,986

Table 3.7: Input values used for TASOPT engine validation.

Variable	Value	Variable	Value
π_{fD}	1.685	α_{\max}	5.103
π_{LPCD}	4.744	f_c	0.19036
π_{HPCD}	3.75	η_{fan}	0.8948
η_b	0.985	η_{LPC}	0.88
G_f	1	η_{HPC}	0.87
\bar{f}_o	0.972	η_{HPT}	0.899
η_{LPT}	0.889	η_{HP}, η_{LP}	0.97
π_{tn}	0.989	π_b	0.94
π_d	0.998	π_{fn}	0.98
W_{engine}	35,008 N		

Table 3.8: TASOPT validation results with engine weight capped at 110% of the TASOPT value, expected to be similar at on design.

Flight Condition	Predicted TSFC [1/hr]	TASOPT TSFC [1/hr]	Percent Difference
Takeoff	0.4751	0.48434	-1.91
Top of Climb	0.7166	0.65290	9.76
On Design	0.6445	0.6404	0.69

Table 3.9: The two operating points used when validating the presented model against the GE90 like NPSS model.

Flight Condition	Altitude [ft]	Mach Number	Thrust [lbf]
TOC	35,000	0.85	19,600
On-Design (cruise)	35,000	0.8	16,408.4

Table 3.10: Input values used for GE90 engine validation

Variable	Value	Variable	Value
π_{fD}	1.58	α_{max}	8.7877
π_{LPCD}	1.26	f_c	0.1444
π_{HPCD}	20.033	η_{fan}	0.9153
η_b	0.997	η_{LPC}	0.9037
G_f	1	η_{HPC}	0.9247
\bar{f}_o	0.955	η_{HPT}	0.9121
η_{LPT}	0.9228	η_{HP}, η_{LP}	0.97
π_{tn}	0.98	π_b	0.94
π_d	0.98	π_{fn}	0.98
W_{engine}	77,399 N		

3.3 NPSS GE90 Validation

The two operating points used for GE90 validation are given in Table 3.9. Again, TOC conditions are similar to cruise conditions, so TSFC discrepancies should be small. The SP model's input values are given in Table 3.10 and results are presented in Table 3.11. TSFC errors are due to assumed gas properties and variations in component maps. This validation case demonstrates that the presented model accurately scales from a CFM56 up to a GE90.

Table 3.11: NPSS GE90 validation results, expected to be similar at both operating points.

Flight Condition	Predicted TSFC [1/hr]	NPSS TSFC [1/hr]	Percent Difference
On Design	0.5328	0.5418	-1.66
TOC	0.5997	0.5876	2.59

Chapter 4

Optimum-Aircraft Parametric Studies

The engine model was integrated with a simplified commercial aircraft sizing model and the combined models were solved to find the aircraft/engine combination that burns the least amount of fuel. The model was solved with a variety of flight profiles as well as a varying number of missions, mission ranges, and minimum climb rates. Effects of these changes on engine sizing and parameter sensitivities are presented. The commercial aircraft sizing model is intentionally simple, capturing only general trends in aircraft sizing. A detailed description of the commercial sizing model is available in Appendix C. For the purposes of this thesis, each mission was discretized into four flight segments - two climb and two cruise. The objective is to minimize total fuel burn. Table 4.1 lists the input values given to the aircraft model. The same engine input values are used as during CFM56 validation (Table 3.3) with the exception of max BPR which is increased to 5.6958, the maximum value from the takeoff, climb, and cruise segments of a TASOPT 737-800 mission. The integrated engine/commercial aircraft sizing model has 628 free variables and solves in 6.78 seconds (6 GP iterations).

Table 4.1: Aircraft sizing and flight profile inputs.

Variable	Value	Unit
N_{eng}	2	-
$W_{S_{\text{max}}}$	6,664	N/m^2
N_{pax}	150	-
e	0.9	-
AR_{max}	10	-

4.1 Optimum-Aircraft Sensitivity to Specified Mission Range

To demonstrate that the combined model captures the proper trends, it was solved for a variety of mission ranges. Each point on the following plots represents a unique aircraft/engine combination. Total fuel burn increased with range, as shown by Figure 4-1.

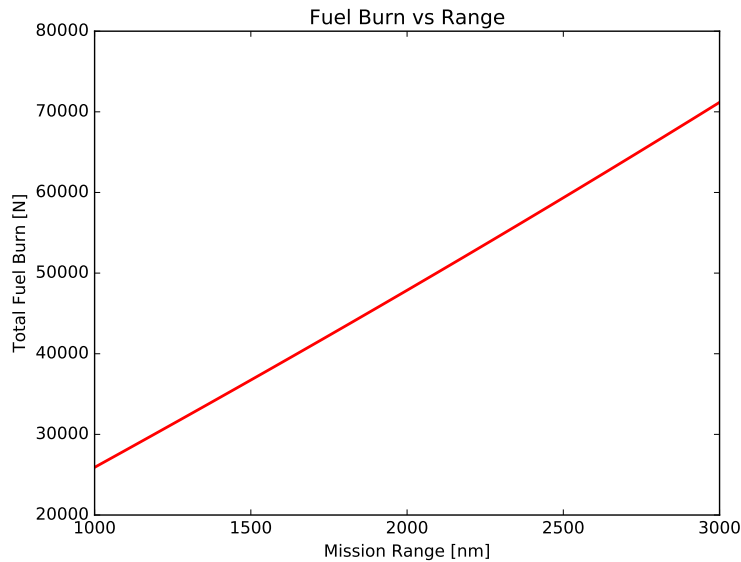
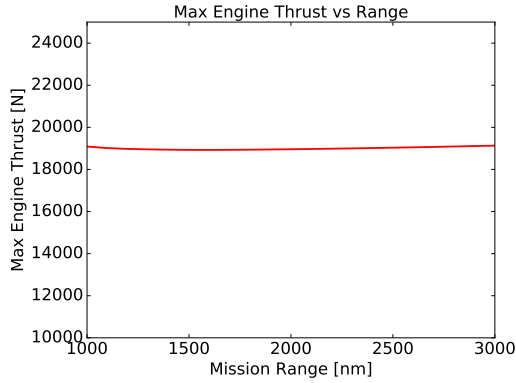


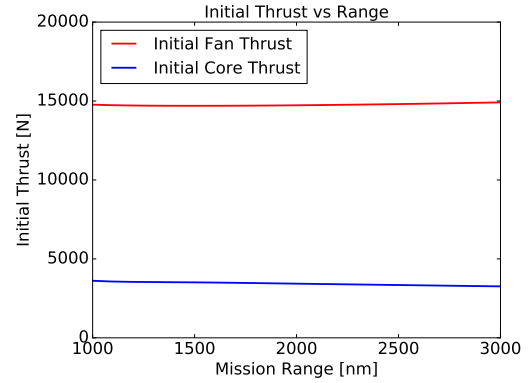
Figure 4-1: Total fuel burn versus mission range.

Figure 4-2 presents plots of max engine thrust, fan and core thrust, initial climb and cruise TSFC, and engine weight versus mission range. All values remain roughly

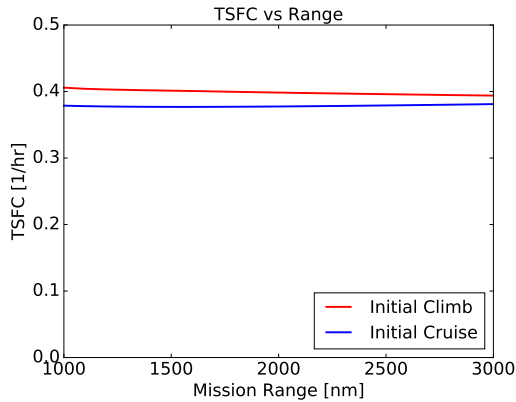
constant across mission range.



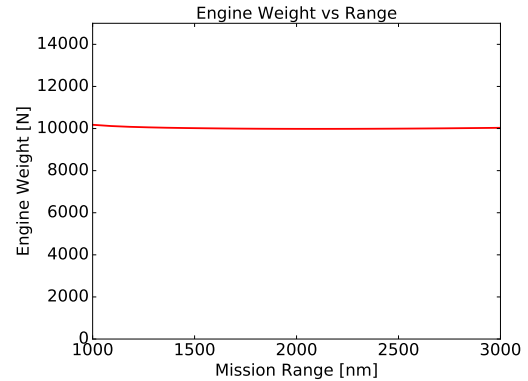
(a) Max engine thrust, which occurs during the initial climb segment, versus mission range.



(b) Fan and core thrust during the initial climb segment versus mission range.



(c) Initial climb and cruise TSFC versus mission range



(d) Engine weight versus mission range.

Figure 4-2: Initial engine thrust, core and fan thrust, climb and cruise TSFC, as well as engine weight for a variety of mission ranges.

4.2 Optimum-Aircraft Sensitivity to Specified Minimum Climb Rate

A minimum initial climb rate constraint was added to shift the nominal design point towards climb. The minimum climb rate was for normal operating conditions (i.e. both engines operating nominally). Increasing the minimum initial climb rate creates a need for increased thrust at low altitude, similar to adding a minimum balanced

field length requirement to an aircraft. The aircraft model was solved across a range of minimum climb rates.

The initial thrust requirement on the engine was larger the higher the minimum climb rate. This is presented in Figure 4-3. The minimum climb rate constraint does not become active until the minimum climb rate exceeds 1,170 ft/min. The total thrust, fan thrust, and core thrust (also plotted in Figure 4-3) all increase in a near linear manner.

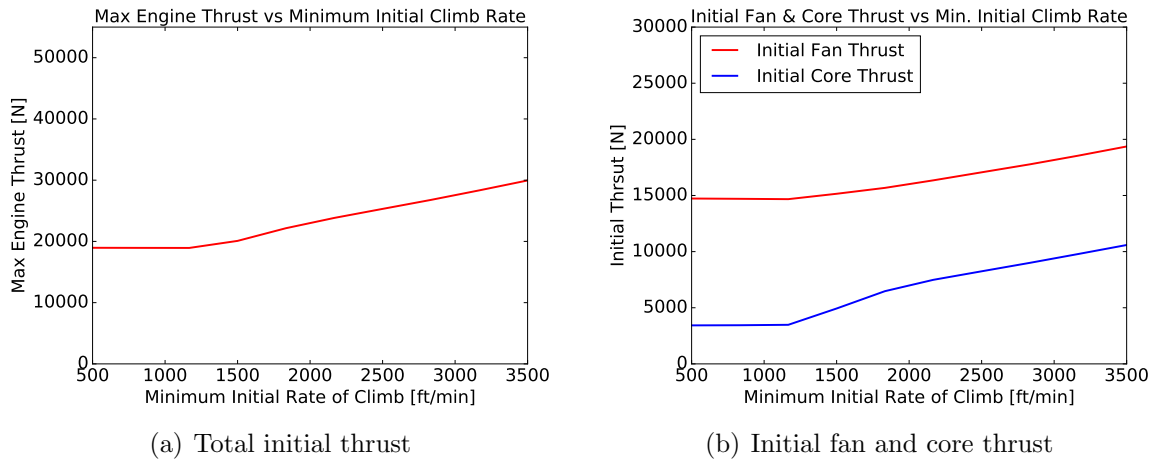


Figure 4-3: Initial fan and core thrust versus minimum initial climb rate.

The engine model predicts engine weight will increase with minimum rate of climb, as shown in Figure 4-4. This is the same as saying engine weight will increase with thrust, which is expected.

As the engine is required to produce more thrust it gets physically larger. Figure 4-5 illustrates this with a plot of fan area versus minimum initial climb rate.

Figure 4-6 presents the initial climb and cruise TSFC versus the minimum initial climb rate. For low minimum initial climb rates, the nominal design point remained at cruise and the cruise TSFC was virtually unaffected by the higher climb rate. However, as the climb rate continued to increase, the design point shifted toward climb and cruise TSFC began to increase. Essentially, the high minimum climb rate requirement is degrading cruise performance. A short balanced field length requirement would degrade the performance of a commercial aircraft in a similar way.

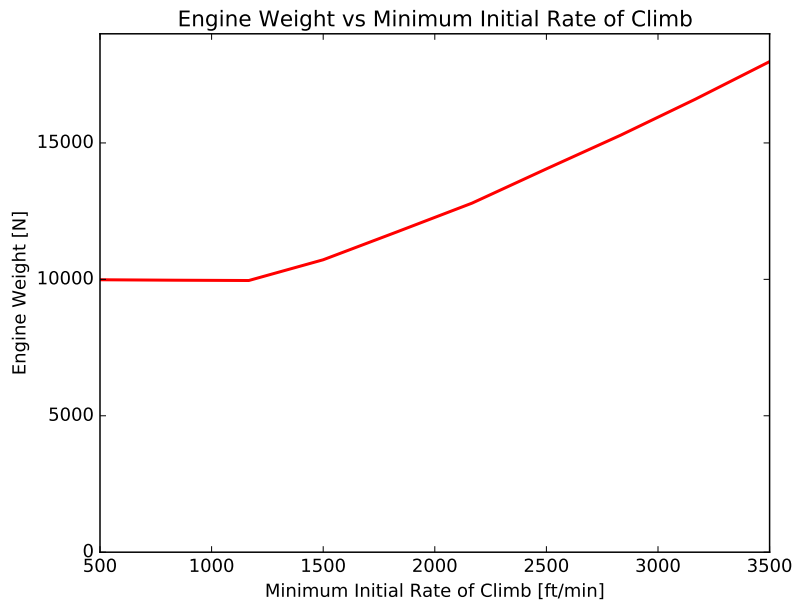


Figure 4-4: Engine weight versus minimum initial climb rate.

4.3 Full Mission Versus Cruise Only Optimization

To illustrate how the removal of the on/off design point distinction allows this thesis’s engine model to select the optimal engine, the climb portion of the flight was removed and the optimal cruise engine was compared to the full mission optimal engine. The aircraft in both missions had the same fuselage area, carried the same payload, and had a cruise range of 2,000 nm. Results are presented in Table 4.2. The nominal design point is shifted towards climb for the full mission engine, causing it to burn 3.37 percent more fuel during cruise than the cruise only engine. All component areas are larger on the cruise only engine, which is (surprisingly) also 41 percent lighter. When climb is not considered, the max thrust requirement and mass flow through the engine are substantially smaller. Consequently, the mass flow dependent data fit engine weight model (Section 2.5) predicts an unrealistically light engine.

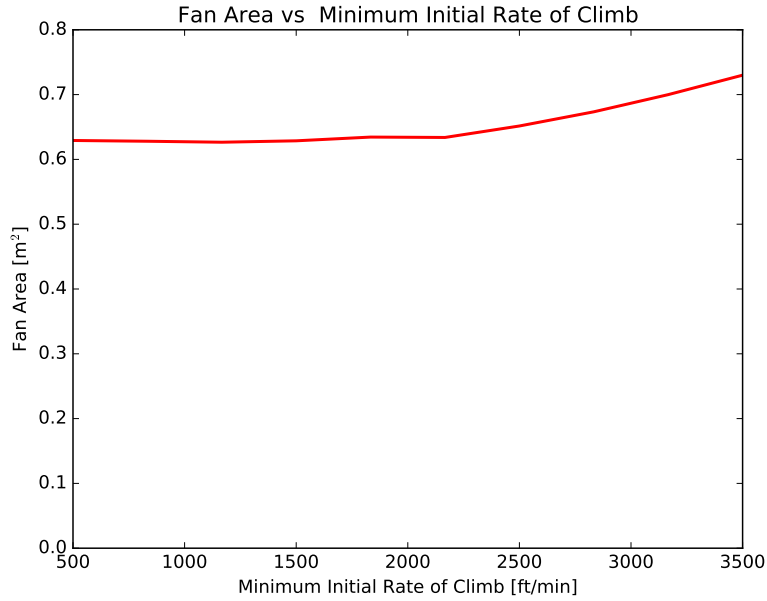


Figure 4-5: Fan inlet area (A_2) versus minimum initial climb rate.

4.4 Multi-Mission Optimization

An extra layer of vectorization was added and the presented engine and simple aircraft model was simultaneously optimized across four missions of ranges 500 nm, 1,000 nm, 1,500 nm, and 2,000 nm. Commercial aircraft are designed for high mission flexibility which degrades overall fuel efficiency, motivating the use of multiple design reference missions when optimizing an aircraft[26]. For simplicity, payload remained constant for each mission. It is assumed the aircraft being optimized will fly 500 nm missions

Table 4.2: Differences in engine size when accounting for the full mission profile and just cruise.

Variable	Full Mission Value	Cruise Only Value	Percent Difference
A_2	0.629 m ²	0.767 m ²	-21.88
A_5	0.205 m ²	0.232 m ²	-13.12
A_7	0.391 m ²	0.472 m ²	-20.65
Engine Weight	9,985.1 N	5,870.4 N	41.21
Initial Cruise TSFC	0.378 1/hr	0.381 1/hr	-1.19

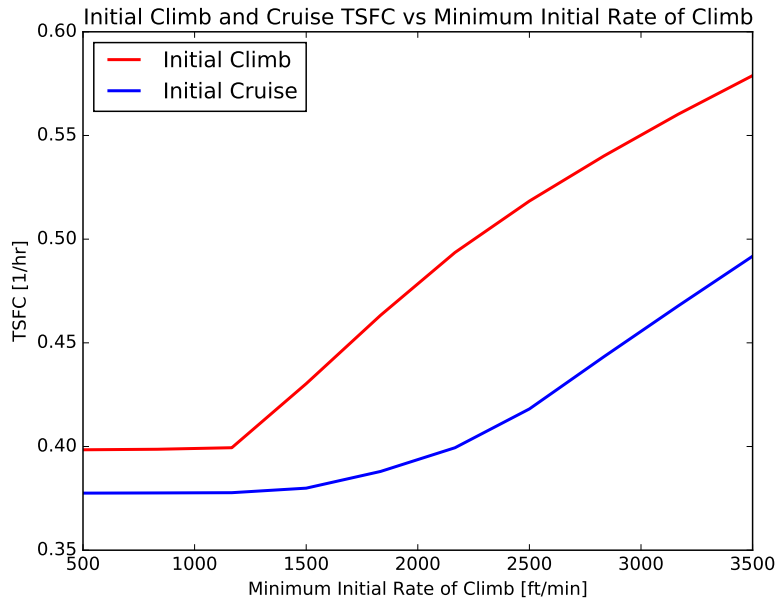


Figure 4-6: Initial climb and cruise TSFC versus minimum initial climb rate.

37.5 percent of the time, 1,000 nm mission 37.5 percent of the time, 1,500 nm missions 12.5 percent of the time, and 2,000 nm missions 12.5 percent of the time. Equation 4.1 is the weighted objective function for this problem.

$$\begin{aligned} \text{objective} = & 0.375W_{\text{fuel}_{500\text{nm}}} + 0.375W_{\text{fuel}_{1,000\text{nm}}} + \\ & 0.125W_{\text{fuel}_{1,500\text{nm}}} + 0.125W_{\text{fuel}_{2,000\text{nm}}} \end{aligned} \quad (4.1)$$

Table 4.3 presents differences in the optimal engine size and fuel burn for the two optimizations. As expected, the multi-mission optimized aircraft burns more fuel during the 2,000 nm mission than the aircraft optimized for just the 2,000 nm flight.

The multi-mission optimization problem has 2,460 free variables and takes 28.3 seconds and six GP iterations to solve.

Table 4.3: Differences in engine size for the presented multi-mission optimization formulation and a single 2,000 nm range mission optimization.

Variable	Single Mission Value	Multi-Mission Value	Percent Difference
A_2	0.629 m ²	0.626 m ²	0.47
A_5	0.205 m ²	0.214 m ²	-3.97
A_7	0.391 m ²	0.403 m ²	-3.17
Engine Weight	9,985.1 N N	10,178.0 N	-1.93
2,000 nm Fuel Burn	47,870 N	48,076 N	-0.43

4.5 Sensitivity Discussion

A strength of convex optimization is that, together with the optimum solution, it provides sensitivities of this solution to all model parameter values. Sensitivities are all local and computed about the optimal point. Equation 4.2[5] is the formula for parameter sensitivities. If the sensitivity to a constant is 0.5 then decreasing that constant by one percent will decrease the objective by approximately one half a percent. If the sensitivity to a constant is -0.75, then a one percent increase in the constant will decrease the objective by approximately three quarters of a percent. Analyzing a model’s sensitivities can be useful in two ways. The first is to determine which areas of a physical design should be improved. For example, if the sensitivity to burner pressure drop is very large, it is advantageous to make the burner pressure drop as small as possible. The second way sensitivities can be used is to guide model development. If the sensitivity to a constant is low, it may not be worthwhile to develop an intricate model for that constant. However, if the sensitivity is large, it is important to ensure it is accurately modeled.

$$\text{Parameter Sensitivity} = \frac{\text{Fractional Objective-Function Change}}{\text{Fractional Parameter Change}} \quad (4.2)$$

The integrated aircraft optimization problem was solved with a mission range of 2,000 nm. Table 4.4 presents a subset of engine sensitivities. The solution is most

Table 4.4: Top engine design value sensitivities in the aircraft optimization example for a single 2,000 nm mission.

Symbol	Description	Sensitivity
\bar{f}_o	1 Minus Percent Mass Flow Bled	-2.50
η_{HPshaft}	High Pressure Shaft Power Transmission Efficiency	-1.50
π_d	Diffuser Pressure Ratio	-1.40
η_b	Combustor Efficiency	-1.10
π_{fn}	Fan Duct Pressure Loss	-1.00
η_{LPshaft}	Low Pressure Shaft Power Transmission Efficiency	-0.86
π_b	Burner Pressure Ratio	-0.39
π_{fD}	On Design Fan Pressure Ratio	0.53

Table 4.5: Top aircraft design and mission parameter sensitivities in the aircraft optimization example.

Variable	Description	Sensitivity
e	Oswald Efficiency Factor	-0.45
W_{pax}	Passenger Weight	0.65
Rng	Required Range	0.94

sensitive to core bleed flow, HP shaft power transmission efficiency, diffuser pressure ratio, combustor efficiency, and the fan duct pressure loss. Increasing any of these values will decrease fuel burn. There is a positive sensitivity to the fan design pressure ratio. Decreasing the fan design pressure ratio will decrease fuel burn.

Table 4.5 presents sensitivities to some of the assumed constants in the aircraft model. Trends are as expected. Increasing the Oswald efficiency factor decreases fuel burn while decreasing passenger weight and mission range decreases fuel burn.

It is also interesting to analyze how sensitivities change as mission parameters change. Figure 4-7 is a plot of the sensitivity to the fan design pressure ratio versus minimum initial climb rate. Initially, it is quite beneficial to decrease the fan design

pressure ratio, as indicated by the sensitivity of approximately 0.53. However, as the minimum climb rate increases and the max thrust requirement on the engine increases, it becomes less beneficial to decrease the fan design pressure ratio. This is indicated by the decrease in sensitivity to approximately 0.1 for a minimum climb rate of 3,500 ft/min.

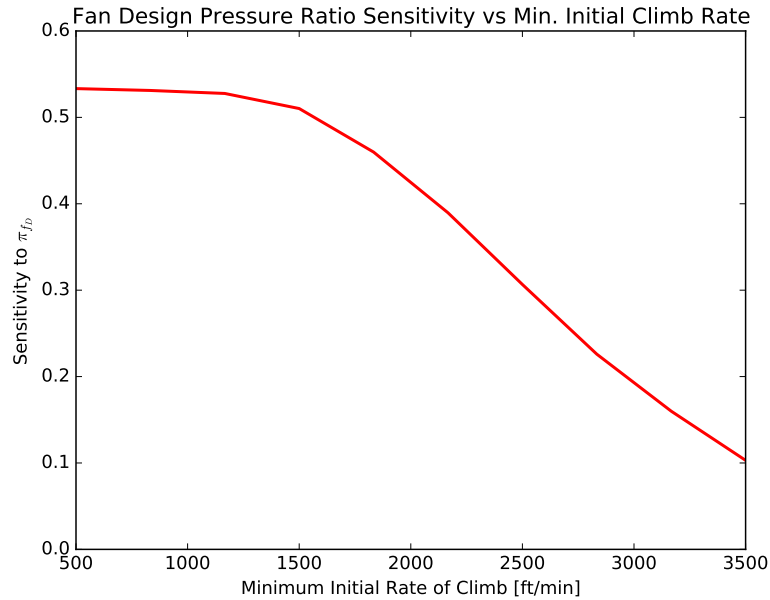


Figure 4-7: Sensitivity to fan design pressure ratio versus minimum initial climb rate.

Chapter 5

Conclusion

This thesis has presented a full 1D core+fan flowpath physics based, signomial programming compatible, turbofan model that was successfully validated against TASOPT and two NPSS models developed by Georgia Tech. The model is meant to be combined with other aircraft subsystem models to perform full system optimization. Using GPKit's performance modeling framework, the turbofan model was formulated as a unified multi-point optimization problem with no on/off design point distinction or order of operations. The model can be easily be integrated into a full aircraft optimization model. This was demonstrated by integrating the turbofan model into a simple commercial aircraft sizing model and performing a series of parametric studies, including a 2,460 variable multi-mission optimization problem that solves in 28 seconds.

Appendix A

Diffuser, Fan, and Compressor Model

Isentropic relations and a free stream Mach number, static pressure, and airspeed are used to constrain inlet stagnation quantities. When the engine model is used as part of a full aircraft optimization model, the ambient atmospheric properties and M_0 are linked to atmosphere and flight profile models. These values are set by the user if the engine is run in isolation. Diffuser boundary layer growth is neglected and a specified diffuser pressure ratio accounts for diffuser stagnation pressure drop. The constraints governing this are presented below. Z_0 replaces the non-GP compatible expression $1 + \frac{\gamma-1}{2}(M_0)^2$ in the stagnation relations.

$$\begin{aligned}
a_0 &= \sqrt{\gamma RT_0} \\
u_0 &= M_0 a_0 \\
P_{t_0} &= P_0 Z_0^{3.5} \\
T_{t_0} &= T_0 Z_0 \\
h_{t_0} &= C_{p_{\text{air}}} T_{t_0} \\
P_{t_2} &= \pi_d P_{t_0} \\
T_{t_2} &= T_{t_0} \\
h_{t_2} &= h_{t_0}
\end{aligned} \tag{A.1}$$

State change across the fan, low pressure compressor (LPC), and high pressure compressor (HPC) are computed using isentropic relations and user specified polytropic efficiencies.

$$\begin{aligned}
P_{t_{i+1}} &= \pi_i P_{t_i} \\
T_{t_{i+1}} &= T_{t_i} \pi_i^{\frac{\gamma_i - 1}{\eta_i \gamma_i}} \\
h_{t_{i+1}} &= C_{p_i} T_{t_i}
\end{aligned} \tag{A.2}$$

Appendix B

Turbine Model

The low pressure turbine (LPT) must supply enough power to drive the fan and LPC. The high pressure turbine (HPT) must supply enough power to drive the HPC. This is ensured by enforcing the two shaft power balance constraints below, both of which are signomial equalities. \bar{f}_o is equal to one minus the percent of mass flow bled to provide pressurization and deice ($1 - \dot{m}_{offtake}/\dot{m}_{core}$). Shaft power offtakes for customer power are smeared into the shaft power transmission efficiencies, $\eta_{HP/LP}$.

$$\bar{f}_o \eta_{HP} (1 + f_f) (h_{t_{4.1}} - h_{t_{4.5}}) = (h_{t_3} - h_{t_{2.5}}), \quad (\text{B.1})$$

$$\bar{f}_o \eta_{LP} (1 + f_f) (h_{t_{4.9}} - h_{t_{4.5}}) = \alpha_{+1} (h_{t_{2.1}} - h_{t_2}) + (h_{t_{1.8}} - h_{t_{2.5}}), \quad (\text{B.2})$$

The isentropic relations and user specified component polytropic efficiencies determine fluid states at stations 4.5 and 4.9.

$$P_{t_{i+1}} = \pi_i P_{t_i} \quad (\text{B.3})$$

$$\pi_i = \left(\frac{T_{t_{i+1}}}{T_{t_i}} \right)^{\frac{\eta_i \gamma_i}{\gamma_i - 1}} \quad (\text{B.4})$$

$$h_{t_{i+1}} = C_{p_i} T_{t_i} \quad (\text{B.5})$$

Appendix C

Flight Profile and Aircraft Sizing Model

The aircraft sizing model and flight profile model sizes a commercial aircraft for minimum fuel burn during a flight of user specified range. The model is discretized into a user selected number of climb and cruise flight segments. Descent is neglected. To avoid introducing a signomial, the downrange distance traveled during climb does not contribute to total mission range.

Basic Aircraft Model Nomenclature

A_{fuse} = projected fuselage area

A_{pax} = required fuselage area per passenger

AR = wing aspect ratio

b = wing span

b_{max} = max allowed wing span

$C_{d_{\text{fuse}}}$ = fuselage drag coefficient

C_{d_w} = wing drag coefficient

D = total aircraft drag

ΔH = altitude change

K = induced drag correction factor

N_{eng} = aircraft's number of engines
 N_{pax} = aircraft's number of passengers
 θ = climb angle
 h = altitude
 L = temperature lapse rate in the troposphere
 P_{excess} = excess power
Range = downrange distance covered
RC = rate of climb
 S = wing planform area
 t = flight segment duration
 V_{stall} = aircraft stall speed
 W_{avg} = average flight segment aircraft weight
 W_{end} = aircraft flight segment end weight
 W_{fuel} = flight segment fuel weight burned
 $W_{\text{fueltotal}}$ = total fuel weight
 W_{fuse} = fuselage weight
 W_{pax} = passenger weight
 W_{payload} = payload weight
 W_{S} = wing loading
 W_{Smax} = max allowed wing loading
 W_{start} = aircraft flight segment start weight
 W_{TO} = takeoff weight
 W_{wing} = wing weight
 z_{bre} = Breguet parameter
 $(\cdot)_{\dots i}$ = flight segment i quantity

C.1 Weight Breakdown

The payload is taken to be only passengers and their baggage. Per passenger total weight (person + baggage) is assumed to be 210 pounds and the number of passengers, N_{pax} , is specified by the user. The empty fuselage and tail weight is approximated as 75 percent of the payload weight. The 75 percent fraction is estimated from TASOPT 737 output. Wing weight is computed using a simplified Raymer wing weight equation normalized by TASOPT 737 wing weight, area, and aspect ratio values[25] in Equation C.3. Total fuel burn is the sum of segment fuel burn.

$$W_{\text{payload}} = W_{\text{pax}} N_{\text{pax}} \quad (\text{C.1})$$

$$W_{\text{fuse}} = 0.75 W_{\text{payload}} \quad (\text{C.2})$$

$$\left(\frac{S}{124.58 \text{m}^2} \right)^{0.65} \left(\frac{AR}{10.1} \right)^{0.5} = \frac{W_{\text{wing}}}{105384.1524 \text{N}} \quad (\text{C.3})$$

$$W_{\text{fuel}_i} = N_{\text{eng}} \text{TSFC}_i t_i F_i \quad (\text{C.4})$$

$$W_{\text{fuel}_{\text{total}}} \geq \sum_{n=1}^N W_{\text{fuel}_i} \quad (\text{C.5})$$

The aircraft's take off weight is the sum of all previously computed weights. Engine weight, W_{eng} , is set by the linked turbofan model. N_{eng} is the user input number of engines.

$$W_{\text{TO}} \geq W_{\text{fuse}} + W_{\text{payload}} + W_{\text{fuel}_{\text{total}}} + N_{\text{eng}} W_{\text{eng}} + W_{\text{wing}} \quad (\text{C.6})$$

Equations C.7 through C.9 set each flight segment's start and end weight.

$$W_{\text{start}_i} = W_{\text{end}_{i-1}} \quad (\text{C.7})$$

$$W_{\text{start}_0} = W_{\text{TO}} \quad (\text{C.8})$$

$$W_{\text{end}_i} \geq W_{\text{empty}} + W_{\text{payload}} + N_{\text{eng}}W_{\text{eng}} + W_{\text{wing}} \quad (\text{C.9})$$

In later constraints, W_{avg_i} , the geometric mean of a segments start and end weight, is used instead of either the segment start or end weight. This increases accuracy and is more stable than using segment start or end weight.

$$W_{\text{avg}_i} = \sqrt{W_{\text{start}_i}W_{\text{end}_i}} \quad (\text{C.10})$$

C.2 Aircraft Sizing

To capture landing/takeoff constraints wing loading is constrained to be less than a user specified max value. Aspect ratio, AR , is set by the wing span and wing area and constrained to be less than a user input maximum value. There is no wing structural model. Without the user input max value aspect ratio would grow unrealistically large.

$$W_{S_i} = \frac{\frac{1}{2}C_{L_i}S\rho_i(V_i)^2}{S} \quad (\text{C.11})$$

$$W_{S_i} \leq W_{S_{\text{max}}} \quad (\text{C.12})$$

$$AR = \frac{b^2}{S} \quad (\text{C.13})$$

$$AR \leq AR_{\text{max}} \quad (\text{C.14})$$

In order to capture trends in fuselage drag, the fuselage is approximated as a flat plate. The plate's area is a function of number of passengers; the area per passenger,

N_{pax} is estimated as $1\text{m}^2/\text{passenger}$. The estimate is based off the per passenger projected fuselage areas of late model 737 and 777s.

$$A_{\text{fuse}} = A_{\text{pax}}N_{\text{pax}} \quad (\text{C.15})$$

The drag coefficient of a turbulent flat plate parallel to the free stream is 0.005. Fuselage drag can then be approximated as $C_{d_{\text{fuse}}} = \frac{1}{2}\rho V^2 A_{\text{fuse}} C_{d_{\text{fuse}}}$ where $C_{d_{\text{fuse}}} = 0.005$.

C.3 General Aircraft Performance

A number of constraints apply to both the climb and cruise portions of the flight. The speed of sound, velocity, and Mach number are computed for each flight segment. Velocity is also constrained to be greater than a user input stall speed. Segment lift, $\frac{1}{2}\rho_i C_{L_i}(V_i)^2$, is equated to the segments average weight.

$$a_i = \sqrt{\gamma R T_i} \quad (\text{C.16})$$

$$V \geq V_{\text{stall}} \quad (\text{C.17})$$

$$V_i = a_i M_i \quad (\text{C.18})$$

$$W_{\text{avg}_i} = \frac{1}{2}\rho_i C_{L_i}(V_i)^2 \quad (\text{C.19})$$

Drag is computed with Equation C.21. The parabolic drag model, with the induced drag parameter K , is used to model induced drag. GPfit[18, 16] was used to develop a GP compatible fit to Xfoil[9] drag data for an NC130 airfoil[10] at a Reynolds number of 20 million. The fit is plotted in Figure C-1. Equation C.20, which sets C_{d_w} , was derived from the data fit.

$$C_{dw} \geq (1.025e10)C_L^{15.58}M^{156.86} + (2.856e-13)C_L^{1.28}M^{6.25} + (2.091e-14)C_L^{0.88}M^{0.03} + (1.944e6)C_L^{5.65}M^{146.52} \quad (C.20)$$

$$D_i \geq \left(\frac{1}{2}\rho_i(V_i)^2\right)(C_{dw} + K(C_L)^2 + C_{D_{\text{fuse}}}A_{\text{fuse}}) \quad (C.21)$$

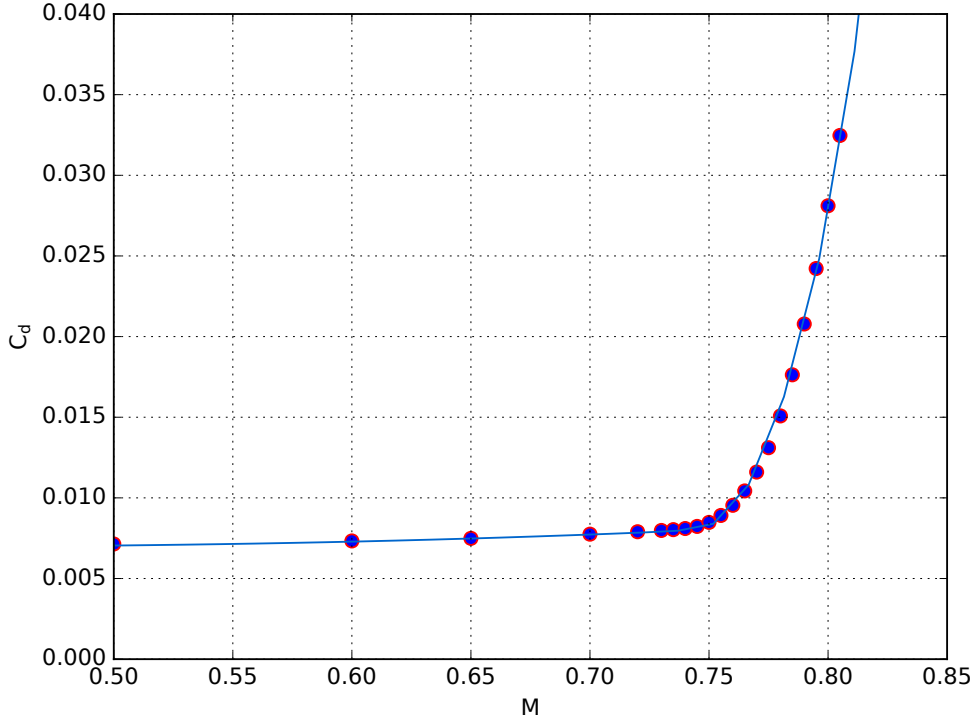


Figure C-1: Xfoil NC130 airfoil drag data (dots) and a posynomial approximation of the data (solid line) for a Reynolds number of 20 million.

$$K = (\pi eAR)^{-1} \quad (C.22)$$

C.4 Climb

The climb rate is set with an excess power formulation[2] and constrained to be greater than 500 ft/min. Equation C.26 uses a small angle approximation to set the climb angle, θ .

$$P_{\text{excess}} + V_i D_i \leq V_i N_{\text{eng}} F_i \quad (\text{C.23})$$

$$\text{RC}_i = \frac{P_{\text{excess}}}{W_{\text{avg}_i}} \quad (\text{C.24})$$

$$\text{RC}_i \geq 500 \text{ ft/min} \quad (\text{C.25})$$

$$\theta_i V_i = \text{RC}_i \quad (\text{C.26})$$

Altitude change during each climb segment is a function of climb rate and total segment time. Equation C.28 uses a small angle approximation to compute the down-range distance covered during a climb segment. This distance is not credited towards the aircraft's mission range.

$$\Delta H_i = t_i \text{RC}_i \quad (\text{C.27})$$

$$t_i V_i = \text{Range}_i \quad (\text{C.28})$$

During climb there is a downward pressure on each segment's end altitude (climbing extra burns more fuel). This allows each climb segments end altitude to be computed with equation C.29.

$$h_i \geq h_{i-1} + \Delta H_i \quad (\text{C.29})$$

C.5 Cruise

During cruise, steady level flight conditions are assumed and segment duration is constrained via equation C.31. This is the same equation as C.28, except it does not use a small angle approximation.

$$D_i = N_{\text{eng}} F_i \quad (\text{C.30})$$

$$t_i V_i = \text{Range}_i \quad (\text{C.31})$$

The Breguet Range equation (Equation C.32) is used to model cruise fuel burn. However, the natural logarithm in Equation C.32 is not GP compatible and must be reformulated using the procedure outlined by Hoburg et al[15]. Equations C.33 and C.34 constitute the reformulated Breguet range equation. W_i in equation C.32 has been replaced with W_{avg_i} to increase accuracy.

$$\ln\left(\frac{W_{\text{start}_i}}{W_{\text{end}_i}}\right) = \frac{D_i(\text{TSFC}_i t_i)}{W} \quad (\text{C.32})$$

$$z_{\text{bre}} + \frac{z_{\text{bre}}^2}{2} + \frac{z_{\text{bre}}^3}{6} \leq \frac{W_{\text{fuel}}}{W_{\text{end}}} \quad (\text{C.33})$$

$$z_{\text{bre}} \geq \frac{D_i(\text{TSFC}_i)}{W_{\text{avg}_i}} t_i \quad (\text{C.34})$$

C.6 Atmosphere Model

Equation C.35, a signomial equality, is used to compute each flight segment's temperature (h is linked to segment end altitude). Atmospheric pressure is computed with the hydrostatic equation and density is computed with the ideal gas law. L_{atm} is the standard temperature lapse rate (0.0065 K/m), R is the universal gas constant, M is

the gasses molar mass, T_{SL} is sea-level temperature, and P_{SL} is the sea level pressure.

$$T_{\text{SL}} = T + L_{\text{atm}}h \quad (\text{C.35})$$

$$\left(\frac{P}{P_{\text{SL}}}\right)^{\frac{LR}{g}} = \frac{T}{T_{\text{SL}}} \quad (\text{C.36})$$

$$\rho = \frac{P}{(R/M)T} \quad (\text{C.37})$$

Appendix D

Signomial Equality Constraint

Intuition

Signomial Equality constraints are required when one variable in a signomial is being pressured in multiple different directions or a posynomial inequality will not remain tight. Consider the constraints used in a simple atmosphere model integrated into an aircraft mission profile. L is the standard the temperature lapse rate of 0.0065 K/m and T_{SL} and P_{SL} are the sea level temperature and pressure, respectively.

$$\rho = \frac{P}{RT}, \quad \left(\frac{P}{P_{\text{SL}}} \right)^{\frac{LR}{g}} = \frac{T}{T_{\text{SL}}}, \quad T_{\text{SL}} = T + Lh \quad (\text{D.1})$$

It is not clear apriori how to relax the posynomial equality $T_{\text{SL}} = T + Lh$ to an inequality. During the climb phase of the flight, there will be an upwards pressure on density (higher density allows a higher climb rate) creating a downwards pressure on T . During the cruise portion of the flight, there will be a downward pressure on density (lower density produces less drag on the aircraft) creating an upwards pressure on T . Situations like this require signomial equality constraints.

Within the engine model, the variables α_{+1} and f_{f+1} are introduced to limit the total number of signomial equalities in the model. Both must be defined via signomial equalities. There is an upward pressure on α (engines with a larger by-pass ratio tend to be more efficient) and α_{+1} due to Equation 2.57, so the GP compatible posynomial

inequality $\alpha_{+1} \geq \alpha + 1$ would not remain tight. Similarly, an upward pressure on f_{f+1} can be generated within the nominal design point estimation constraints in Section 2.2 so the constraint $f_{f+1} \geq f + 1$ would not remain tight.

$$\alpha_{+1} = \alpha + 1 \tag{D.2}$$

$$f_{f+1} = f_f + 1 \tag{D.3}$$

Appendix E

Engine Boundary Layer Ingestion

An engine boundary layer ingestion (BLI) model is required to model the D8. The D8 engine configuration is illustrated in Figure E-1. BLI engines ingest air with lower average velocity, and in turn lower stagnation pressure, than free stream air. The following analysis assumes the engine will ingest half free stream and half boundary layer air, in line with current BLI propulsor research[14].

Three constraints were modified to account for BLI. Equation A.1 was replaced by Equation E.1 where inlet stagnation pressure is reduced by the factor f_{BLIP} . Note f_{BLIP} represents the average drop in stagnation pressure across the entire inlet, i.e., if the boundary layer has on average 40 percent less stagnation pressure than f_{BLIP} would be set to 0.2.

$$P_{t_0} = f_{\text{BLIP}} P_{\text{atm}} Z_0^{3.5} \quad (\text{E.1})$$

Thrust is equal to the working fluid's rate of momentum change. The factor

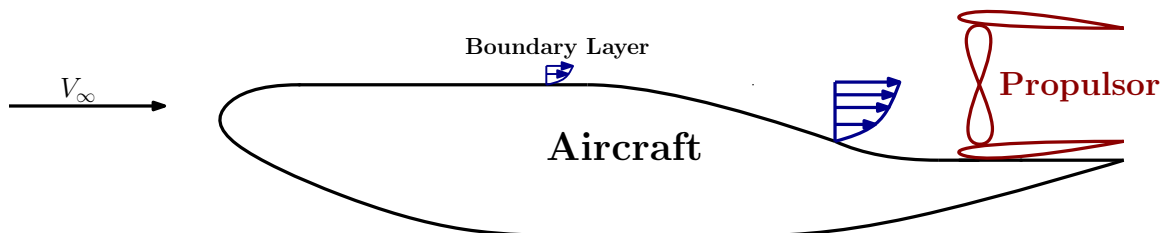


Figure E-1: Cartoon illustrating boundary layer growth on a BLI equipped aircraft similar to the D8.

f_{BLIV} was introduced to fan and core thrust constraints (Equations 2.53 and 2.54) to account for the decrease in average free stream velocity. Again, f_{BLIV} is the average velocity drop across the entire fan.

$$F_8/(\alpha\dot{m}_{\text{core}}) + f_{\text{BLIV}}u_0 \leq u_8 \quad (\text{E.2})$$

$$F_6/(\bar{f}_o\dot{m}_{\text{core}}) + f_{\text{BLIV}}u_0 \leq u_6 \quad (\text{E.3})$$

Determining f_{BLIP} and f_{BLIV} can be difficult. As of now, there are no GP or SP compatible boundary layer models so either f_{BLIP} or f_{BLIV} must be estimated. One method of estimation is to assume a boundary layer profile, such as Falkner-Skan. This could apply to a flat plate (including a flat plate at an angle of attack)[11]. In practice this has proven inaccurate, particularly for high speed boundary layers. If an estimate for the boundary layer's kinetic energy defect is available, it is possible to estimate f_{BLIP} via a mass weighted average of entropy as shown in TASOPT[10]. This method is applicable to high speed boundary layers. Finally, it is possible to estimate f_{BLIP} from the experimental results presented by Hall et al.[8]. After estimating either f_{BLIP} or f_{BLIV} , the other can be determined using Equation E.4.

$$f_{\text{BLIP}} = \frac{P_{\text{atm}} + 0.5\rho_{\text{atm}}(f_{\text{BLIV}}\text{Ma})^2}{P_{\text{atm}} + 0.5\rho_{\text{atm}}(\text{Ma})^2} \quad (\text{E.4})$$

It is important to note fan distortion effects will decrease fan efficiency to approximately 90%[3].

Bibliography

- [1] <https://www.cfmaeroengines.com/engines/cfm56/>.
- [2] John D Anderson. *Aircraft Performance and Design*. WCB McGraw-Hill, Boston, Massachusetts, 1999.
- [3] V. Madani D. Crichton E.M. Greitzer T.P. Hynes C.A. Hall A.P. Plas, M.A. Sargeant. Performance of a boundary layer ingesting (bli) propulsion system. *AIAA Aerospace Sciences Meeting and Exhibit*, 2007.
- [4] ApS. The mosek c optimizer api manual, 2015. Version 7.1 (Revision 41).
- [5] Stephen Boyd, Seung-Jean Kim, Lieven Vanderberghe, and Arash Hassibi. A tutorial on geometric programming. *Optim Eng*, 2007.
- [6] Stephen Boyd and Lieven Vandenberghe. *Convex Optimization*. Cambridge University Press, The address, 7 edition, 2009.
- [7] Edward Burnell and Warren Hoburg. Gpkit software for geometric programming. <https://github.com/hoburg/gpkit>, 2015. Version 0.4.0.
- [8] C.S. Tan D.K. Hall, E.M. Greitzer. Analysis of fan stage desing attributes for boundary layer ingestion. *ASME Turbo Expo*, 2016.
- [9] Mark Drela. Xfoil: An analysis and design system for low reynolds number airfoils. In *Low Reynolds Number Aerodynamics*, pages 1–12. Springer, 1989.
- [10] Mark Drela. N3 aircraft concept designs and trade studies - appendix. technical report nasa cr-2010-216794/vol2. Technical report, NASA, 2010.
- [11] Mark Drela. *Aerodynamics of Viscous Flows*. Cambridge, MA, draft edition, 2015.
- [12] R.J Duffin, E.L. Peterson, and C. Zener. *Geometric programming: theory and application*,. Wiley New York, 1967.
- [13] GeneralElectric. Energy efficient engine flight propulsion system aircraft/engine integration evaluation. Technical report, NASA, 1980.
- [14] David Hall. *Analysis of Civil Aircraft Propulsors with Boundary Layer Ingestion*. PhD thesis, Massachussets Institute of Technology, 2 2015.

- [15] Warren Hoburg and Pieter Abbeel. Geometric programming for aircraft design optimization. *AIAA Journal*, 2014.
- [16] Warren Hoburg, Philippe Kirschen, and Pieter Abbeel. Data fitting with geometric-programming-compatible softmax functions. *Optim Eng*, 2016.
- [17] Southwest Research Institute. Numerical propulsion system simulation. <http://www.swri.org/npss/purchase.asp>.
- [18] Philippe Kirschen and Warren Hoburg. Gpfit. <https://github.com/convexopt/gpfit>, 2015. Version 0.1.
- [19] Philippe G. Kirschen, Edward E. Burnell, and Warren W. Hoburg. Signomial programming models for aircraft design. *AIAA SciTech*, 2016.
- [20] Thomas Lipp and Stephen Boyd. Variations and extension of the convex concave procedure. *Optim Eng*, 2015.
- [21] Joaquim R.R. Martins and Andrew B. Lambe. Multidisciplinary design optimization: A survey of architectures. *AIAA Journal*, 2013.
- [22] D. Marvis. Environmental design space (eds) overview. Technical report, Presentation to the Transportation Research Board, Papers and Briefings on the Development Program for the Aviation Environmental Tool Suite, Workshop no. 4, Dec. 6-8, 2006, URL: http://www.faa.gov/about/office_org/headquarters_offices/apl/research/models/history/media/05_DM_Overview-EDS_2006-11-28_FINAL.pdf, 2010.
- [23] Exxon Mobil. Jet fuel product properties. <https://www.exxonmobil.com/English-FI/Commercial-Fuel/pds/GLXXJetFuel-Series>.
- [24] Max M.J. Opgenoord, Brian S. Cohen, and Warren W. Hoburg. Equality constraints for signomial programming. *Optim Eng*, 2016.
- [25] Daniel P. Raymer. *Aircraft Design: A Conceptual Approach*. American Institute of Aeronautics and Astronautics, Reston, Virginia, 4th edition, 2006.
- [26] Brian Yutko. *The Impact of Aircraft Design Reference Mission on Fuel Efficiency in the Air Transportation System*. PhD thesis, Massachusetts Institute of Technology, 10 2013.